JACS
JOURNAL OF THE AMERICAN CHEMICAL SOCIETY
Article
pubs.acs.org/JACS

Tuning the Quinoid versus Biradicaloid Character of Thiophene-Based Heteroquaterphenoquinones by Means of Functional Groups

Eleonora V. Canesi,*[,†] Daniele Fazzi,[†] Letizia Colella,[†,‡] Chiara Bertarelli,[‡] and Chiara Castiglioni[‡]

[†]Center for Nano Science and Technology @PoliMi, Istituto Italiano di Tecnologia, Via Pascoli 70/3, 20133 Milano, Italy
[‡]Dipartimento di Chimica, Materiali e Ing. Chimica "G. Natta", Politecnico di Milano, Piazza L. Da Vinci 32, 20133 Milano, Italy

Supporting Information

ABSTRACT: A series of quinoidal bithiophenes (QBTs) with controlled variations in steric hindrance and electron activity of the substituents has been synthesized. Evidence of their quinoidal versus biradicaloid ground-state electronic character has been experimentally detected and coherently identified as fingerprints by spectroscopic methods such as NMR, UV–vis, multiwavelength Raman. From this analysis, alkoxy groups have been shown to strongly affect the electronic structure and the ground-state energy and stability of QBTs. Quantum-chemical calculations correctly predict the experimental spectroscopic response, even while changing the alkyl on phenone from a tertiary carbon atom to secondary to primary toward an unsubstituted phenone, further confirming the validity of the approach proposed. A control of the electronic structure accompanied by negligible variations of the optical gap of the molecules has thus been demonstrated, extending the potential use of quinoidal species in fields ranging from photon harvesting to magnetic applications.

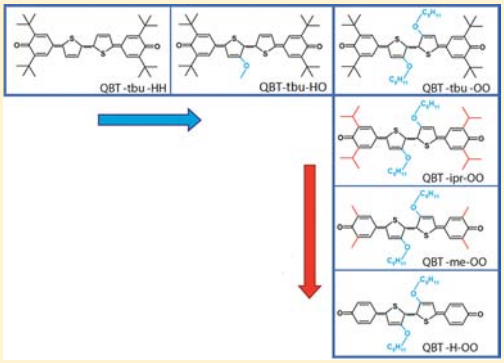

INTRODUCTION

Thiophene-based quinoidal molecules[1−6] have found a renewed interest in the literature,[7−9] especially due to their amphoteric redox character and high electron affinity,[3] which confer on them air stability and an ambipolar or n-type electronic behavior.[4,10,11]

Recently, an unexpected biradicaloid character was shown to occur in thiophene quinoidal derivatives, which is favored by increasing the length of the conjugated cores; by combining theoretical and experimental approaches, Raman spectroscopy has been lately demonstrated to be a suitable technique to probe the electronic structure of quinoidal species.[7−9,12] The monitoring, in terms of frequency shifts and intensity variations, of those Raman active normal modes that are sensitive to π-electron delocalization (in particular the so-called Я-modes, corresponding to collective vibrations that maximize the electron−phonon coupling interaction)[13] has been revealed as a powerful tool to discriminate different highly π-conjugated compounds on the basis of the character of their ground electronic state (i.e., quinoid vs biradicaloid). In the case of thiophene-based heterophenoquinones, it has been found that by increasing the molecular chain length, a strong red shift (80−120 cm^{-1}) of the Я-mode frequency is observed until a turning point, where the Я-mode starts to blue-shift.[9] This behavior has been rationalized in terms of modulation of the equilibrium molecular structure, while going from a quinoidal structure (as obtained by density functional theory (DFT) closed-shell (CS) calculations) for short-length molecules to a more aromatic-like (e.g., biradicaloid) structure (predicted by DFT broken symmetry (BS) calculations) for longer systems.[8,9]

Parallel to the intriguing ground-state properties of quinoidal compounds, excited states have been investigated as well, both theoretically (time-dependent DFT, TDDFT, and CASSCF//CASPT2 calculations) and experimentally (UV–vis and PL). The presence of a low-lying double exciton state responsible for the weak features in the high wavelength region of their absorption spectra was observed, thus highlighting a possible use of these materials for up- or down-conversion processes such as singlet fission and triplet–triplet annihilation.[14−17]

Accordingly, we expect that the ground/excited-state electronic characters could be tuned not only by increasing the molecular length but also by the presence and nature of functional groups bound to the conjugated chain. Tuning the electronic character without affecting to a large extent the degree of π electrons conjugation is of interest: indeed, a separate control of the two characteristics (quinoid vs biradicaloid structure and excited-state energies) allows the independent choice of the optical bandgap and the electronic structure of the ground state. Specifically, longer molecules are usually characterized by intense absorption in the red and near-infrared spectral region[6] and are interesting for photodetection in telecommunication[18] as well as low bandgap species for photovoltaics.[19] However, biradicaloid structures enable isomerization,[20] which, in principle, could be responsible for instability and lower charge mobility;[21,22] in addition, the accessibility to dark states is expected to influence the molecular optical response, in terms both of lifetime and of

Received: July 24, 2012
Published: October 22, 2012

   dx.doi.org/10.1021/ja3072385 | J. Am. Chem. Soc. 2012, 134, 19070−19083

intensity of absorptive and emissive transitions. On the other hand, open-shell species are studied for third-order nonlinear optical properties[23] and for magnetic applications,[24] thanks to their nonvanishing electron spin resonance signals: accordingly, the presence of such peculiar properties also on shorter oligomers can be of interest as well. A reliable characterization of the electronic structure is thus of great relevance, because it can draw the guidelines for the design of new quinoidal derivatives.

In this work, we present a series of novel symmetric and asymmetric thiophene-based heteroquaterphenoquinones, which differ in the alkyl in the 3,5-positions of the phenoquinones and bearing electron-active groups on the bithiophene core. With respect to benzoquinoidal species, thienoquinoidal oligomers can be easily synthesized, due to their higher stability, and the versatility of the chemistry of thiophene gives access to its functionalization.[20] 5,5′-Bis(3,5-di-*tert*-butyl-4-oxo-2,5-cyclohexadiene-1-ylidene)-5,5′-dihydro-2,2′-bithiophene (QBT-tbu-HH in Figure 1), whose biradicaloid nature has been recently investigated,[8,14] was considered as the reference species. In the design of new derivatives, we considered functional groups affecting the chemical-physical properties that are commonly addressed for the application requirements, such as the solubility, the supramolecular ordering at the solid state, and the energy levels of the frontier molecular orbitals. Different experimental techniques (NMR, UV−vis, IR, Raman with different excitation wavelengths), supported by quantum chemical calculations (DFT, TDDFT, CASSCF), were used to characterize the new species, aiming (i) at determining the influence of the substituents on the stabilization of a predominant quinoidal or a biradicaloid ground state structure and (ii) at studying the different interplay between excited states. For each spectroscopic technique, experimental markers related to the electronic structure of the investigated species are highlighted.

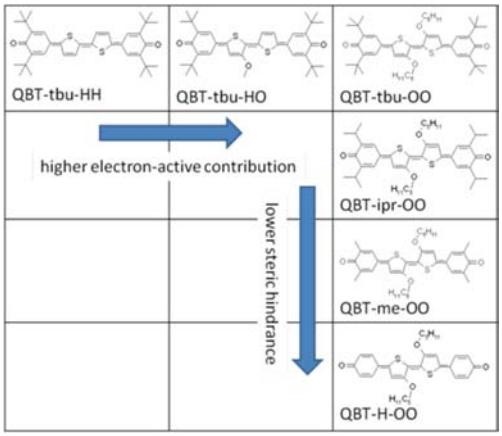

Figure 1. Chemical structures of the molecules under investigation, listed by increasing number of alkoxy chains (row) and decreasing steric hindrance of end units (column).

MATERIALS AND METHODS

Apparatus. ^{1}H NMR and ^{13}C NMR spectra were collected through a Bruker ARX 400. Mass spectroscopy has been carried out with a Bruker Esquire 3000 plus. UV−vis absorption spectra were recorded on a Cary 5000 spectrophotometer (Varian). Electrochemical measurements were carried out by cyclic voltammetry (CV) by using an Autolab PGSTAT 30 potentiostat of Eco-Chemie (Utrech, The Netherlands), run by a PC with the NOVA 1.8 software. The working electrode was a 0.071 cm^2 glassy carbon GC disk embedded in Teflon (Amel, IT), and the counter electrode was platinum wire. Aqueous saturated calomel (SCE) was used as operating reference electrode, in a double bridge containing a CH_2Cl_2 + 0.1 M tetrabutylammonium perchlorate (TBAP) solution, to avoid water and KCl pollution of the working solution. (Details on cyclic voltammetry measurements are reported in the Supporting Information.)

FT infrared spectra were collected on a Nicolet NEXUS FTIR spectrometer. Raman spectra were recorded with (i) a Nicolet FT-Raman Nexus NXR 9650, which employs a Nd/YAG laser with excitation at λ = 1064 nm, and (ii) a Horiba Jobin Ivon Labram HR800 equipped with a microscope, using 514.5 and 632 nm excitation lines. Thermal evolution of the Raman spectra was analyzed by using the Horiba Jobin Ivon Labram HR800 (excitation 514.5 nm, nominal power 100 uW) on solid samples, collecting and averaging two scans with 1 cm^{-1} spectral resolution.

Synthesis and Electrochemical Characterization. Unless otherwise specified, all reagents, catalysts, spectroscopic grade, and reagent grade solvents were commercial (Sigma Aldrich). All reactions of air- and water-sensitive reagents and intermediates were performed in dried glassware under argon. The solvents were previously dried by conventional methods and stored under argon. Air- and water-sensitive solutions were transferred with hypodermic syringes or double-ended needles.

General Procedure for the Preparation of Tris[3,5-di(alkyl)-4-(trimethylsilyloxy)phenyl]boroxine. Butyllithium (2.5 M in hexane, 1.1 equiv) was added dropwise to a stirred suspension of 4-bromo-2,6-dialkylphenol trimethylsilyl ether[25] (1 equiv) in dry TMEDA/THF (v/v 1:8) at −78 °C. After 1 h at −78 °C, B(O-iPr)$_3$ (3 equiv) was added, and the resulting solution was stirred at −78 °C for 45 min. The mixture was stirred overnight, while being allowed to warm to room temperature. Saturated aqueous NH_4Cl solution was added, and the reaction mixture was extracted with dichloromethane (DCM). The organic layer was dried on Na_2SO_4, and the solvent was removed under reduced pressure. The product was purified using flash chromatography (silica gel). **(a) Tris[3,5-di-*tert*-butyl-4-(trimethylsilyloxy)phenyl]boroxine (1):** 4-Bromo-2,6-di-*tert*-butylphenol trimethylsilyl ether (2 g, 5.6 mmol), THF (20 mL), TMEDA (4 mL), BuLi 2.5 M (8.4 mmol), B(O-iPr)$_3$ (5.2 mL, 22.4 mmol). Flash chromatography using petroleum benzine/ethyl acetate 2:1 afforded the desired compound as a yellow solid in 66% yield. ^{1}H NMR (400 MHz; $CDCl_3$, 25 °C, TMS): δ 8.194 (s, 6H; H_2,H_6 phenyl), 1.516 (s, 54H; *tert*-butyl), 0.471 ppm (s, 27H; −OSiMe$_3$). **(b) Tris[3,5-di-iso-propyl-4-(trimethylsilyloxy)phenyl]boroxine (2):** 4-Bromo-2,6-di-iso-propylphenol trimethylsilyl ether (4.118 g, 12,5 mmol), THF (60 mL), TMEDA (8 mL), BuLi 2.5 M (12.5 mmol), B(O-iPr)$_3$ (37.5 mmol). Flash chromatography using petroleum benzine/ethyl acetate 2:1 afforded the desired product as a yellowish solid in 55% yield. ^{1}H NMR (400 MHz; $CDCl_3$, 25 °C, TMS): δ 7.973 (s, 6H; H_2,H_6 phenyl), 3.296 (hept, ^3J(H,H) = 6.840 Hz, 6H; −CH iso-propyl), 1.301 (d, ^3J(H,H) = 6.840 Hz, 36H; −CH$_3$ iso-propyl), 0.314 ppm (s, 27H; −OSiMe$_3$). The material typical contains ∼20% of the corresponding boronic acid. ^{1}H NMR (400 MHz; $CDCl_3$, 25 °C, TMS): δ 7.432 (s, 2H; H_2,H_5 phenyl), 3.296 (m, 2H; −CH iso-propyl), 1.221 (d, ^3J(H,H) = 6.840 Hz, 12H; −CH$_3$ iso-propyl), 0.277 ppm (s, 9H; −OSiMe$_3$).

2-Bromo-3-methoxythiophene (3). A solution of *N*-bromosuccinimide (3.11 g, 17.5 mmol) in dry DMF (12 mL) has been added dropwise in a solution of 3-methoxythiophene (2 g, 17.5 mmol) in dry DMF (8 mL). After 1 h, the reaction mixture was extracted with DCM, the organic layer was dried on Na_2SO_4, and the solvent was removed under reduced pressure. Flash chromatography using petroleum benzine/DCM 9:1 afforded the desired product as a transparent liquid in 88% yield. ^{1}H NMR (400 MHz; $CDCl_3$, 25 °C, TMS): δ 7.200 (d, J = 5.9 Hz, 1H; H_5 thiophene), 6.760 (d, J = 5.2 Hz, 1H; H_4 thiophene), 3.889 ppm (s, 3H; −O−CH$_3$).

3-Methoxy-2,2′-bithiophene (4). A solution of 2-bromothiophene (1.4 g, 8.5 mmol) in dry diethyl ether (5 mL) was added dropwise to a

dx.doi.org/10.1021/ja3072385 | J. Am. Chem. Soc. 2012, 134, 19070−19083

stirred suspension of magnesium turnings (0.3 g, 12.3 mmol) in dry diethyl ether (10 mL). After 2 h at reflux, the mixture was cooled to room temperature, dropped into a stirred solution of 2-bromo-3-methoxythiophene (1.5 g, 7.7 mmol) and $NiCl_2$(dppp) (0.424 g, 0.77 mmol) in dry diethyl ether (30 mL), and refluxed for 10 h. After an overnight stirring at room temperature, the reaction mixture was quenched with ice and an aqueous solution of HCl (2M) and extracted with diethyl ether/H_2O. The organic layer was dried over Na_2SO_4, and the solvent was removed under reduced pressure. The product was purified using silica gel flash chromatography with petroleum benzine/DCM 9:1 to give the desired product as a yellow liquid in 88% yield. ^{1}H NMR (400 MHz; $CDCl_3$, 25 °C, TMS): δ 7.217 (dd, $^3J(H_{3'},H_{4'})$ = 3.6 Hz, $^3J(H_{3'},H_{5'})$ = 1 Hz, 1H; $H_{3'}$ thiophene), 7.182 (dd, $^3J(H_{5'},H_{4'})$ = 5.0 Hz, $^3J(H_{5'},H_{3'})$ = 1 Hz, 1H; $H_{5'}$ thiophene), 7.045 (d, ^3J(H,H) = 5.6 Hz, 1H; H_5 thiophene), 6.992 (dd, $^3J(H_{4'},H_{3'})$ = 3.6 Hz, $^3J(H_{4'},H_{5'})$ = 5.3 Hz, 1H; $H_{4'}$ thiophene), 6.85 (d, ^3J(H,H) = 5.6 Hz, 1H; H_4 thiophene), 3.993 ppm (s, 3H; $-OCH_3$).

General Procedure for the Preparation of 5,5′-Dibromo-3,3′-R_1,R_2-2,2′-bithiophene. To a solution of 3,3′-R_1,R_2-2,2′-bithiophene (1 equiv) in dry DMF was added dropwise *N*-bromosuccinimide (2 equiv) in dry DMF, in the absence of light. After 1 h, the reaction mixture was extracted with DCM and washed with water. The organic layer was dried over Na_2SO_4, and the solvent was removed under reduced pressure. The product was purified using flash chromatography (silica gel). **(a) 5,5′-Dibromo-3-methoxy-2,2′-bithiophene (6):** 3-Methoxy-2,2′-bithiophene (1 g, 5 mmol) in DMF (10 mL), *N*-bromosuccinimide (1.78 g, 10 mmol) in DMF (10 mL). Flash chromatography in petroleum benzine/DCM 9:1 afforded the desired product as a light green solid in 74% yield. ^{1}H NMR (400 MHz; $CDCl_3$, 25 °C, TMS): δ 6.915 (d, ^3J(H,H) = 3.6 Hz, 1H; $H_{3'}$ thiophene), 6.85 (s, 1H; H_4 thiophene), 6.81 (d, ^3J(H,H) = 3.6 Hz, 1H; $H_{4'}$ thiophene), 3.993 ppm (s, 3H; $-OCH_3$). **(b) 5,5′-Dibromo-3,3′-dipentoxy-2,2′-bithiophene (7):** 3,3′-Dipentoxy-2,2′-bithiophene[26] (1.5 g, 4.44 mmol) in DMF (20 mL), *N*-bromosuccinimide (1.74 g, 9.76 mmol) in DMF (10 mL). Flash chromatography using petroleum benzine/DCM 3:1 afforded the desired product as a yellow solid in 72% yield. ^{1}H NMR (400 MHz; $CDCl_3$, 25 °C, TMS): δ 6.811 (s, 2H; H_4,$H_{4'}$ thiophene), 4.039 (t, ^3J(H,H) = 6.539 Hz, 4H; $-OCH_2-$), 1.836 (m, 4H; $-CH_2-$), 1.481 (m, 4H; $-CH_2-$), 1.409 (m, 4H; $-CH_2-$), 0.948 ppm (t, ^3J(H,H) = 7.193 Hz, 6H; $-CH_3$).

General Procedure for the Preparation of 5,5′-Bis(3,5-dialkyl-4-hydroxy)phenyl-3,3′-R_1,R_2-2,2′-bithiophene. To a solution of 5,5′-dibromo-3,3′-R_1,R_2-2,2′-bithiophene (1 equiv) and $Pd(PPh_3)_4$ (0.1 equiv) in previously degassed DME (2:1 with respect to water) were rapidly added boronic acid (2.5 equiv) or boroxine (1 equiv) and aqueous base solution (9 eq, 1 M). The resulting mixture was refluxed overnight. Next, it was allowed to cool to room temperature, poured into water, and extracted with diethyl ether or DCM. The organic layer was dried over Na_2SO_4, and, after solvent removal, the raw product was purified using flash chromatography (silica gel). **(a) 5,5′-Bis-(3,5-di-*tert*-butyl-4hydroxy)phenyl-2,2′-bithiophene (11):** 5,5′-Dibromo-2,2′-bithiophene (0.413 g, 1.276 mmol), $Pd(PPh_3)_4$ (0.147 g, 0.1276 mmol), tris[3,5-di-*tert*-butyl-4-(trimethylsilyloxy)phenyl]boroxine (1.165 g, 1.276 mmol), Na_2CO_3 solution (11.5 mL, 11.484 mmol). Flash chromatography with petroleum benzine/DCM 9:1 afforded the desired product as a yellow solid in 87% yield. ^{1}H NMR (400 MHz; $CDCl_3$, 25 °C, TMS): δ 7.414 (s, 4H; H_2,H_6 phenyl), 7.123 (d, ^3J(H,H) = 3.8 Hz, 2H; H_3,$H_{3'}$ thiophene), 7.086 (d, ^3J(H,H) = 3.8 Hz, 2H; H_4,$H_{4'}$ thiophene), 5.278 (s, 2H; −OH), 1.491 ppm (s, 36H; *tert*-butyl). **(b) 5,5′-Bis-(3,5-di-*tert*-butyl-4-hydroxy)phenyl-3-methoxy-2,2′-bithiophene (12):** 5,5′-Dibromo-3-methoxy-2,2′-bithiophene (0.530 g, 1.5 mmol), $Pd(PPh_3)_4$ (0.170 g, 0.15 mmol), tris[3,5-di-*tert*-butyl-4-(trimethylsilyloxy)phenyl]boroxine (0.9 g, 1.0 mmol), Na_2CO_3 solution (13.5 mL, 13.5 mmol). Flash chromatography using petroleum benzine/DCM 9:1 afforded the desired product as a yellow solid in 75% yield. ^{1}H NMR (400 MHz; $CDCl_3$, 25 °C, TMS): δ 7.418 (s, 2H; −H phenyl), 7.384 (s, 2H; −H phenyl), 7.175 (d, ^3J(H,H) = 3.8 Hz, 1H; $H_{3'}$ thiophene), 7.074 (d, ^3J(H,H) = 3.8 Hz, 1H; $H_{4'}$ thiophene), δ 6.984 (s, 1H; H_4 thiophene), 5.227 (s, 2H; −OH), 4.016 (s, 3H; $-OCH_3$), 1.429 ppm (s, 36H; *tert*-butyl). **(c) 5,5′-Bis-(3,5-di-*tert*-butyl-4-hydroxy)phenyl-3,3′-dipentoxy-2,2′-bithiophene (13):** 5,5′-Dibromo-3,3′-dipentoxy-2,2′-bithiophene (0.200 g, 0.403 mmol), $Pd(PPh_3)_4$ (0.046 g, 0.04 mmol), tris[3,5-di-*tert*-butyl-4-(trimethylsilyloxy)phenyl]boroxine (0.348 g, 0.403 mmol), $NaHCO_3$ solution (5 mL, 5 mmol). Flash chromatography using petroleum benzine/ethyl acetate 95:5 afforded **13** as a light green solid in 33% yield. ^{1}H NMR (400 MHz; DMSO, 25 °C, TMS): δ 7.354 (s, 4H; −H phenyl), 7.267 (s, 2H; −OH), 7.106 (s, 2H; H_4,$H_{4'}$ thiophene), 4.202 (t, J(H,H) = 6.32 Hz, 4H; $-OCH_2$), 1.822 (m, 4H; $-CH_2-$), 1.604 (m, 4H; $-CH_2-$), 1.429 (s, 36H; *-tert*-butyl), 1.398 (m, 4H; $-CH_2-$), 0.929 ppm (t, ^3J(H,H) = 7.411 Hz; $-CH_3$). **(d) 5,5′-Bis-(3,5-di-iso-propyl-4-hydroxy)phenyl-3,3′-dipentoxy-2,2′-bithiophene (14):** 5,5′-Dibromo-3,3′-dipentoxy-2,2′-bithiophene (0.318 g, 0.64 mmol), $Pd(PPh_3)_4$ (0.500 g, 0.64 mmol), tris[3,5-di-iso-propyl)-4-(trimethylsilyloxy)phenyl]boroxine (0.750 g, 0.06 mmol), $NaHCO_3$ solution (6 mL, 5.76 mmol). Flash chromatography using petroleum benzine/ethyl acetate 9:1 afforded **14** as a light green solid in 43% yield. ^{1}H NMR (400 MHz; DMSO, 25 °C, TMS): δ 8.282 (s, 2H; −OH), 7.325 (s, 2H; H_4,$H_{4'}$ thiophene), 7.247 (s, 4H; −H phenyl), 4.212 (t, ^3J(H,H) = 5.883 Hz, 4H; $-OCH_2$), 3.327 (m, 4H; −CH iso-propyl), 1.827 (m, 4H; $-CH_2-$), 1.627 (m, 4H; $-CH_2-$), 1.447 (m, 4H; $-CH_2-$), 1.210 (d, ^3J(H,H) = 6.986 Hz, 24H; −CH3 iso-propyl), 0.950 ppm (t, ^3J(H,H) = 7.354 Hz, 6H; $-CH_3$). **(e) 5,5′-Bis-(3,5-dimethyl-4-hydroxy)phenyl-3,3′-dipentoxy-2,2′-bithiophene (15):** 5,5′-Dibromo-3,3′-dipentoxy-2,2′-bithiophene (0.320 g, 0.645 mmol), $Pd(PPh_3)_4$ (0.750 g, 0.065 mmol), 4-hydroxy-3,5-dimethylphenyl boronic acid pinacol ester (0.400 g, 1.613 mmol), $NaHCO_3$ solution (6 mL, 5.8 mmol). Flash chromatography using petroleum benzine/ethyl acetate 2:1 afforded **15** as a light green solid in 60% yield. ^{1}H NMR (400 MHz; DMSO, 25 °C, TMS): δ 7.254 (s, 2H; H_4,$H_{4'}$ thiophene), 7.199 (s, 4H; −H phenyl), 4.176 (t, ^3J(H,H) = 5.883 Hz, 4H; $-OCH_2$), 2.195 (s, 12H; $-CH_3$ phenyl), 1.812 (m, 4H; $-CH_2-$), 1.573 (m, 4H; $-CH_2-$), 1.433 (m, 4H; $-CH_2-$), 0.959 ppm (t, ^3J(H,H) = 7.383 Hz, 6H; $-CH_3$ pentoxy). **(f) 5,5′-Bis-(4-hydroxy)phenyl-3,3′-dipentoxy-2,2′-bithiophene (16):** 5,5′-Dibromo-3,3′-dipentoxy-2,2′-bithiophene (1 g, 2.016 mmol), $Pd(PPh_3)_4$ (0.233 g, 0.2 mmol), 4-hydroxyphenylboronic acid (0.8346 g, 6.048 mmol), $NaHCO_3$ solution (18 mL, 18.145 mmol). Flash chromatography using petroleum benzine/ethyl acetate 2:1 afforded **16** as a green powder in 66% yield. ^{1}H NMR (400 MHz; DMSO, 25 °C, TMS): δ 7.447 (d, ^3J(H,H) = 8.719 Hz, 4H; H_2,H_6 phenyl), 7.278 (s, 2H, H_4,$H_{4'}$ thiophene), 6.8 (d, ^3J(H,H) = 8.719 Hz, 4H; H_3,H_5 phenyl), 4.173 (t, ^3J(H,H) = 6.321 Hz, 4H; $-OCH_2$), 1.812 (m, 4H; $-CH_2-$), 1.533 (m, 4H; $-CH_2-$), 1.412 (m, 4H; $-CH_2-$), 0.930 ppm (t, ^3J(H,H) = 7.411 Hz, 6H; $-CH_3$).

General Procedure for the Preparation of 5,5′-Bis-(3,5-R_3,R_3-4-oxo-2,5-cyclohexadiene-1-ylidene)-3,3′-R_1,R_2-2,2′-dihydroxy Bithiophene. To a solution of 5,5′-bis-(3,5-R_3,R_3-4-hydroxy)phenyl-3,3′-R_1,R_2-2,2′-bithiophene (1 equiv) in DCM were added $K_3Fe(CN)_6$ (10 equiv) and an aqueous solution of KOH (100 equiv, 0.3 M). The resulting mixture was stirred until the starting material completely reacted (~3 h). The reaction mixture was extracted with DCM and washed with water. Solvent removal afforded the desired product in quantitative yield. **(a) 5,5′-Bis-(3,5-di-*tert*-butyl-4-oxo-2,5-cyclohexadiene-1-ylidene)-2,2′-dihydroxy Bithiophene (QBT-tbu-HH):** 5,5′-Bis-(3,5-di-*tert*-butyl-4-hydroxy)phenyl-2,2′-bithiophene (0.641 g, 1.115 mmol, 75 mL), $K_3Fe(CN)_6$ (3.67 g, 11.15 mmol), aqueous KOH solution (6.25 g, 111.5 mmol, 150 mL). The product was isolated as a green solid. ^{1}H NMR (400 MHz; $CDCl_3$, 25 °C, TMS): δ 7.530 (s, 2H; H thiophene), 7.415 (d, ^3J(H,H) = 5 Hz, 4H; H_2,H_6 phenyl), 7.246 (s, 2H; H thiophene), 1.369 ppm (s, 36 H; *-tert*-butyl). HRMS (ESI): *m*/*z* calcd for $C_{36}H_{44}O_2S_2$+H^+, 573 [M + H^+]; found, 573.3 (M^+). FT-IR (KBr, cm^{-1}): 1575, 1484, 1452, 1359, 1323, 1026, 989. **(b) 5,5′-Bis-(3,5-di-*tert*-butyl-4-oxo-2,5-cyclohexadiene-1-ylidene)-3-methoxy-2,2′-dihydroxy Bithiophene (QBT-tbu-HO):** 5,5′-Bis-(3,5-di-*tert*-butyl-4-hydroxy)phenyl-3-methoxy-2,2′-bithiophene (0.250 g, 0.44 mmol), DCM (75 mL), $K_3Fe(CN)_6$ (1.7 g, 5 mmol), aqueous KOH solution (2.8 g, 50 mmol, 150 mL). The product is isolated as an iridescent green/red solid. ^{1}H NMR (400 MHz; $CDCl_3$, 25 °C, TMS): δ 7.407 (d, 2H; H phenyl), 7.329 (s, 2H; H phenyl),

Scheme 1. Synthetic Route for QBTs

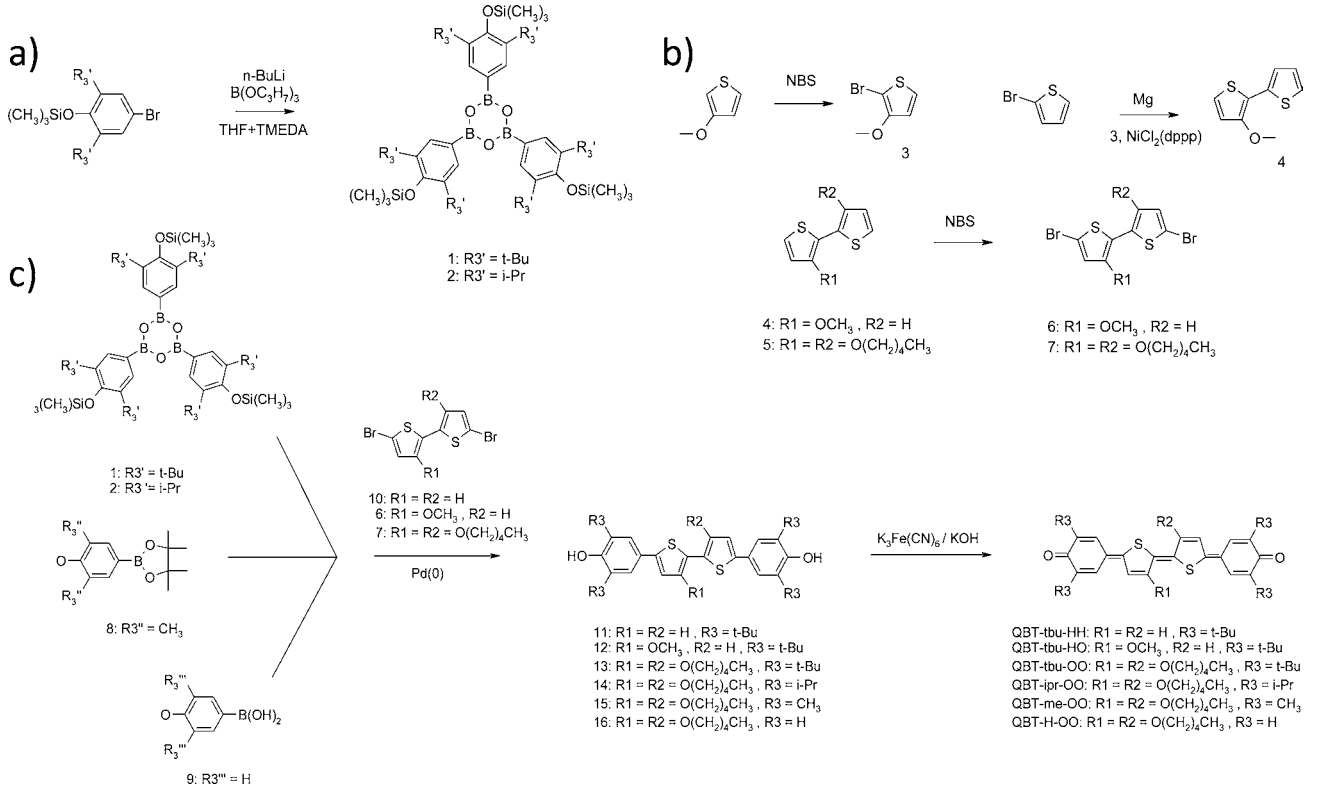

7.229 (s, 2H; $H_{3'}$,$H_{4'}$ thiophene), 6.768 (s, 1H; H_4 thiophene), 4.1 (s, 3H; $-OCH_3$), 1.367 ppm (s, 36H; *-tert*-butyl). HRMS (ESI): *m/z* calcd for $C_{37}H_{46}O_3S_2 + H^+$, 603 [M + H^+]; found, 603.3 (M^+). FT-IR (KBr, cm^{-1}): 1582, 1529, 1487, 1451, 1358, 1329, 1257, 1237, 1088, 1025, 988. **(c) 5,5′-Bis-(3,5-di-*tert*-butyl-4-oxo-2,5-cyclohexadiene-1-ylidene)-3,3′-dipentoxy-2,2′-dihydroxy Bithiophene (QBT-tbu-OO):** 5,5′-Bis-(3,5-di-*tert*-butyl-4-hydroxy)phenyl-3,3′-dipentoxy-2,2′-bithiophene (0.050 g, 0.067 mmol) in DCM (23 mL), $K_3Fe(CN)_6$ (0.22 g, 0.67 mmol), aqueous KOH solution (0.375 g, 6.7 mmol, 17 mL). The product was isolated as a purple/blue solid. ^{1}H NMR (400 MHz; $CDCl_3$, 25 °C, TMS): δ 7.323 (d, ^4J(H,H) = 2.409 Hz, 2H; −H phenyl), 7.307 (d, ^4J(H,H) = 2.409 Hz, 2H; −H phenyl), 6.775 (s, 2H; H_4,$H_{4'}$ thiophene), 4.279 (t, ^3J(H,H) = 5.889 Hz, 4H; $-OCH_2$), 1.99 (m, 4H; $-CH_2-$), 1.640 (m, 4H; $-CH_2-$), 1.465 (m, 4H; $-CH_2-$), 1.362 (s, 18H; *-tert*-butyl), 1.353 (s, 18H; *-tert*-butyl), 0.981 ppm (t, ^3J(H,H) = 7.228 Hz, 6H; $-CH_3$). APT NMR (300 MHz; $CDCl_3$): δ 185.261 (C), 163.934 (C), 152.105 (C), 125.949 (C), 122.135 (C), 106.845 (CH), 73.083 (CH_2), 35.626 (C), 35.545 (C), 29.731 (CH_3), 28.769 (CH_2), 23.3 (CH_2), 22.322 (CH_2), 13.967 (CH_3). HRMS (ESI): *m/z* calcd for $C_{46}H_{64}O_4S_2 + H^+$, 745 [M + H^+]; found, 745.5 (M^+). FT-IR (KBr, cm^{-1}): 1578, 1531, 1491, 1452, 1357, 1331, 1232, 1088, 1026, 988. **(d) 5,5′-Bis-(3,5-di-iso-propyl-4-oxo-2,5-cycloesadiene-1-ylidene)-3,3′-dipentoxy-2,2′-dihydroxy Bithiophene (QBT-ipr-OO):** 5,5′-Di (3,5-di-iso-propil-4-hydroxy)phenyl-3,3′-dipentoxy-2,2′-bithiophene (0.060 g, 0.087 mmol) in DCM (30 mL), $K_3Fe(CN)_6$ (0.286 g, 0.87 mmol), aqueous KOH solution (0.487 g, 8.7 mmol, 22 mL). The product was isolated as a dark blue solid. ^{1}H NMR (400 MHz; $CDCl_3$, 25 °C, TMS): δ 7.273 (d, ^4J(H,H) = 2H; −H phenyl), 7.247 (d, ^4J(H,H) = 2H; −H phenyl), 6.853 (s, 2H; H_4,$H_{4'}$ thiophene), 4.333 (t, ^3J(H,H) = 5.951 Hz, 4H; $-OCH_2$), 3.288 (m, 4H; −CH iso-propyl), 2.033 (m, 4H; $-CH_2-$), 1.880 (m, 4H; $-CH_2-$), 1.680 (m, 4H; $-CH_2-$), 1.204 (d, ^3J(H,H) = 4.883 Hz, 12H; −CH3 iso-propyl), 1.187 (d, ^3J(H,H) = 4.883 Hz, 12H; −CH3 iso-propyl), 1.014 ppm (t, ^3J(H,H) = 7.324 Hz, 6H; $-CH_3$). APT NMR (300 MHz; $CDCl_3$): δ 183.867 (C), 164.136 (C), 152.409 (C), 126.273 (C), 122.688 (C), 107.1 (CH), 73.236 (CH_2), 35.626 (C), 28.749 (CH_2), 28.337 (CH_2), 27.082 (CH), 22.387 (CH_2), 22.234 (CH_3), 14.003 (CH_3). HRMS (ESI): *m/z* calcd for $C_{42}H_{56}O_4S_2 + H^+$, 689 [M + H^+]; found, 689.4 (M^+). FT-IR (KBr, cm^{-1}): 1565, 1531, 1486, 1459, 1407, 1350, 1250, 1104, 1077, 984. **(e) 5,5′-Bis-(3,5-dimethyl-4-oxo-2,5-cyclohexadiene-1-ylidene)-3,3′-dipentoxy-2,2′-dihydroxy bithiophene (QBT-me-OO):** 5,5′-Bis-(3,5-dimethyl-4-hydroxy)phenyl-3,3′-dipentoxy-2,2′-bithiophene (0.225 g, 0.389 mmol) in DCM (132 mL), $K_3Fe(CN)_6$ (1.279 g, 3.89 mmol), aqueous KOH solution (2.178 g, 38.9 mmol, 97 mL). The product was isolated as a dark blue solid. ^{1}H NMR (400 MHz; $CDCl_3$, 25 °C, TMS): δ 7.339 (d, 4H; −H phenyl), 6.844 (s, 2H; H_4,$H_{4'}$ thiophene), 4.308 (t, ^3J(H,H) = 5.955 Hz, 4H; $-OCH_2$), 2.131 (s, 12H; $-CH_3$ phenyl), 2.021 (m, 4H; $-CH_2-$), 1.672 (m, 4H; $-CH_2-$), 1.433 (m, 4H; $-CH_2-$), 1.047 ppm (t, ^3J(H,H) = 7.443 Hz, 6H; $-CH_3$). HRMS (ESI): *m/z* calcd for $C_{34}H_{40}O_4S_2 + H^+$, 577 [M + H^+]; found, 577.2 (M^+). FT-IR (KBr, cm^{-1}): 1574, 1534, 1486, 1469, 1409, 1371, 1336, 1267, 1196, 1171, 1067, 1048, 1036, 964. **(f) 5,5′-Bis-(4-oxo-2,5-cyclohexadiene-1-ylidene)-3,3′-dipentoxy-2,2′-dihydroxy Bithiophene (QBT-H-OO):** 5,5′-Bis-(4-hydroxy)phenyl-3,3′-dipentoxy-2,2′-bithiophene (0.400 g, 0.763 mmol) in DCM (270 mL), $K_3Fe(CN)_6$ (2.510 g, 7.63 mmol), aqueous KOH solution (4.273 g, 76.3 mmol, 190 mL). The product was isolated as a dark blue solid. ^{1}H NMR (400 MHz; $CDCl_3$, 25 °C, TMS): δ 7.530 (dd, J(H,H) = 9.997 Hz, 4H; H_2,H_6 phenyl), 6.853 (s, 2H; H_4,$H_{4'}$ thiophene), 6.511 (dd, J(H,H) = 9.997 Hz, 4H; H_3,H_5 phenyl), 4.320 (t, ^3J(H,H) = 6.051 Hz, 4H; $-OCH_2$), 2.022 (m, 4H; $-CH_2-$), 1.616 (m, 4H; $-CH_2-$), 1.480 (m, 4H; $-CH_2-$), 1.009 ppm (t, ^3J(H,H) = 7.23 Hz; $-CH_3$). HRMS (ESI): *m/z* calcd for $C_{30}H_{32}O_4S_2 + H^+$, 521 [M + H^+]; found, 521.2 (M^+). FT-IR (KBr, cm^{-1}): 1614, 1599, 1577, 1533, 1481, 1410, 1354, 1259, 1164, 1025, 966.

Computational Methods. Density functional theory (DFT) quantum chemical calculations have been carried out for the whole series of molecules sketched in Figure 1. Different exchange-correlation (XC) DFT functionals has been considered using the hybrid Becke's three-parameters B3LYP[27] and range-separated CAM-B3LYP[28] coupled to a double split Pope basis set, 6-31G**. All of the optimized molecular structures are in a stable minimum of the ground state potential, and no imaginary frequencies have been computed.

dx.doi.org/10.1021/ja3072385 | J. Am. Chem. Soc. 2012, 134, 19070−19083

Table 1. HOMO−LUMO Energies, HOMO−LUMO Energy Gap Derived from the Electrochemical Data ($E^{\text{HOMO-LUMO}}_{(\text{exp})}$), and Energy Gap Theoretically Predicted ($E_{\text{GAP(theo)}}$[a])

compound	HOMO_{exp} [eV]	LUMO_{exp} [eV]	$E^{\text{HOMO-LUMO}}_{(\text{exp})}$ [eV]	$E_{\text{GAP(theo)}}$ [eV]
QBT-tbu-HH	−5.086	−3.954	1.132	1.682 (BS)
QBT-tbu-HO	−5.047	−3.922	1.125	1.643 (BS)
QBT-tbu-OO	−4.905	−3.836	1.069	1.615

[a]Computed values are at the (U)B3LYP/6-31G** (S_0-CS) and (S_0-BS) level; see Materials and Methods.

As was already reported in other studies,[3,8,9] the stability of the ground state DFT wave-function has been tested by the keyword *stable=opt*. For those cases where the ground-state closed-shell (S_0-CS) DFT wave-function result to be unstable, a full geometry reoptimization at the unrestricted UDFT level has been carried out, computing the equilibrium structure for the corresponding ground-state broken symmetry (S_0-BS) DFT wave-function. For both B3LYP and CAM-B3LYP functionals, the S_0-CS and S_0-BS cases have been considered for each molecule featuring a biradicaloid character. For the case of QBT-H-OO, a complete-active space SCF calculation CASSCF featuring 12 active electrons in 12 molecular orbitals (CASSCF-(12,12)) has been carried out with the 6-31G* basis set. Excited-state calculations have been carried out at the time-dependent TD-DFT level by using both B3LYP and CAM-B3LYP functional. Vertical excitation energies and oscillator strengths have been computed for each molecule. For the case of QBT-H-OO and QBT-H−OH, the molecular structure of the singlet dipole allowed excited state (S_2) has been fully optimized. Excited-state force field for S_2 state has been computed. Franck−Condon factors have been evaluated (B3LYP and CAM-B3LYP), as widely reported in literature (notice that due to the computational cost, tbu groups have been replaced by H in these calculations).[29−37] Medium effects have been considered by computing, for both ground and excited states, the equilibrium geometries and force fields using the IEFPCM method[38,39] (solvent = chloroform). Negligible effects have been observed. All calculations have been carried out by using the Gaussian 09 package.[40] The ground-state CASSCF(12,12)/6-31G* calculation for QBT-H-OO has been performed with NWChem code.[41]

RESULTS AND DISCUSSION

Synthesis. All of the molecules synthesized in this work (Figure 1) are obtained by chemical oxidation of phenol end-capped bithiophene skeletons, where the quinoid character is induced by the terminal carbonyl groups. Without side groups, the molecule is almost insoluble in common organic solvents. For this reason, introduction of lateral substituents can play the double role of increasing solubility and tuning the electronic properties. Two different positions of the conjugated skeleton have been considered, and substituents have been systematically varied to yield homologous series of compounds, as follows: (i) alkyl chains on the 3,5-positions of phenone, *tert*-butyl (tbu), iso-propyl (ipr), methyl (me), and, as reference, hydrogen (H); and (ii) alkoxy on the 3,3′ positions of the bithienylene core. Molecules are labeled as QBT-(x)-Y where (x) indicates the alkyl groups on phenone (tbu, ipr, me, H) and Y refers to the presence of alkoxy groups; specifically Y = OO means the substitution on both the 3,3′ positions of bithiophene, whereas Y = HO is used when the molecule bears just one alkoxy group. Molecules synthesized are summarized in Figure 1, where the systematic variation of the molecular structure is highlighted.

Because functionalities are linked to two different parts of the molecule, the synthetic scheme proceeded by preparing the homologous phenol end-capping groups (**1**, **2**, **8**, and **9**, Scheme 1a) and the thienylenes (**6**, **7**, and **10**, Scheme 1b), which were then coupled following a combinatorial approach (Scheme 1c).

As was recently reported,[8] Suzuki coupling between a 5,5′-dibromo-bithiophene and a *para*-phenol boronic acid or anhydride is the most effective reaction to yield aromatic phenol end-capped α,α'-thienylenes. Regarding phenols bearing bulky *tert*-butyl or iso-propyl groups, boronic derivatives are not commercially available, and tris-phenyl boroxine precursors (**1**and **2**), which are characterized by high stability, solubility, and easy purification run, were prepared. Symmetric 3,3′-dipentoxy-2,2′-bithiophene has been synthesized according to the published procedure,[26] and further brominated with NBS in DMF. For asymmetric 3-methoxy-2,2′-bithiophene, a Kumada coupling between 2-bromo-3-methoxy thiophene, obtained from bromination of 3-methoxy thiophene with NBS, and the freshly prepared Grignard reagent of 2-bromothiophene was carried out. The Suzuki coupling between the functionalized 5,5′-dibromo-2,2′-bithiophenes and the benzene boronic derivatives gave the aromatic precursors of QBTs, which were subsequently oxidized with potassium ferricyanide to yield the target molecules.

All of the synthesized species are soluble enough to be characterized by solution techniques. However, as expected, we observed a reduction of solubility by moving along the vertical arrow of Figure 1, that is, by going from *tert*-butyl to less steric demanding groups (ipr→me), to unsubstituted phenoquinone. In particular, QBT-H-OO shows a solubility of just a few mg/ml in chlorinated solvents. These findings are quite surprising if we consider that relatively long alkoxy chains are present that were supposed to contribute to the solubility of the material. However, it is worth noting that alkoxy chains at the 3,3′-positions of bithiophene do not cause distortion of the molecular structure due to a possible interaction between the lone pairs of sulfur and oxygen,[20] and/or to the partial double bond character of the central CC bond. This may favor a strong intermolecular packing at the solid state.

On the other hand, the length of the alkoxy chain was expected not to significantly influence the electronic features of the molecules (this hypothesis would be further confirmed by calculations, see below); for this reason, in QBT-tbu-HO, methoxy has not been converted to pentoxy, with *tert*-butyls guaranteeing good solubility.

Details on the synthetic procedures and on characterization methods are reported in the Materials and Methods.

The effect of the presence of donor alkoxy groups on the frontier energy levels was first investigated through cyclic voltammetry. Table 1 summarizes the energies of the frontier molecular orbitals of QBT-tbu-HH, QBT-tbu-HO, and QBT-tbu-OO, derived using the Fc^+/Fc couple as a standard according to the following equations:

$$E_{\text{HOMO}}\ (\text{eV}) = -e\cdot[E_{\text{p,a}}(\text{V vs } Fc^+|Fc) + 4.8(\text{V } Fc^+|Fc \text{ vs zero})] \quad (1)$$

dx.doi.org/10.1021/ja3072385 | J. Am. Chem. Soc. 2012, 134, 19070−19083

$$E_{LUMO}\ (eV) = -e\cdot[E_{p,c}(V \text{ vs } Fc^{+}|Fc) + \\ + 4.8(V\ Fc^{+}|Fc \text{ vs zero})] \quad (2)$$

where e corresponds to the number of exchanged electrons, while E is the peak potential (anodic or cathodic, taken with the maxima criterion).

As expected, the presence of the alkoxy groups raises both the energy of the HOMO level and that of the LUMO. However, the LUMO energy is less affected, thus resulting in a progressive reduction of the HOMO−LUMO energy gap going from QBT-tbu-HH to QBT-tbu-OO. Computed DFT values nicely fit the trend of the experimental energy gap.

NMR spectroscopy provided interesting features about the structure of quinoidal species: molecule QBT-tbu-HH is known to be characterized by broad ^{1}H NMR signals (Figure 2).[1,42]

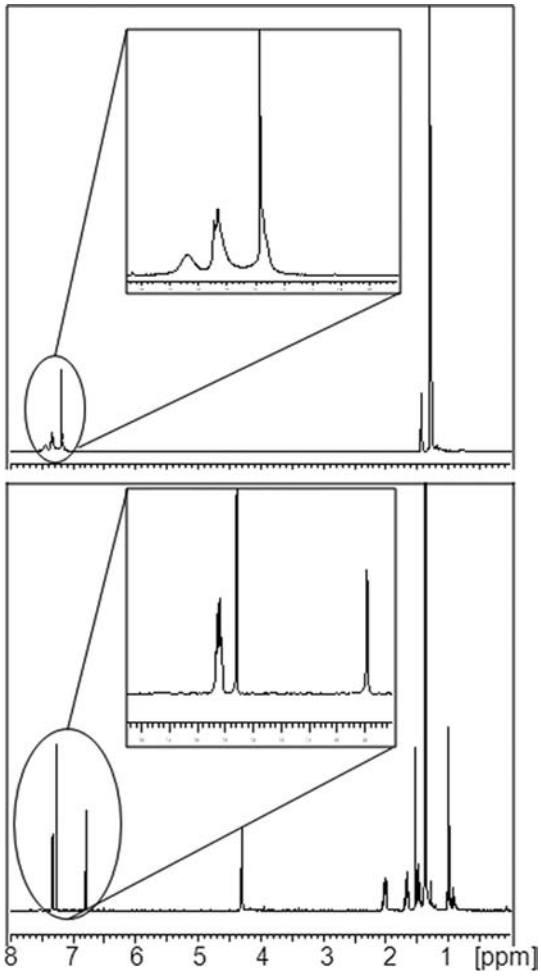

Figure 2. ^{1}H NMR spectra of QBT-tbu-HH (top) and QBT-tbu-OO (bottom) in $CDCl_3$.

Takahashi rationalized these spectroscopic features (and also of analogous heteroquaterphenoquinones; see ref 1) by dynamic ^{1}H NMR spectroscopy, clarifying that QBT exists predominantly in an *S-trans* conformation in $CDCl_3$ solution with a relative ratio between the *S-trans* and the *S-cis* of 2.23:1 at −40 °C. Coalescence of the NMR signals of the two conformers has been indeed observed starting from 10 °C. Markedly different evidence has been detected for QBT-tbu-OO (Figure 2), which is characterized by well-defined ^{1}H NMR peaks at room temperature. A significant shift of the signals of protons on thiophenes, which move from 7.2−7.5 ppm down to 6.8 ppm going from QBT-tbu-HH to QBT-tbu-OO, is also observed, as a result of the deshielding caused by the vicinal oxygen atoms.

Conversely, the alkyl substitution onto the phenoquinone produces a negligible effect on the magnetic spectroscopic response of the aromatic nuclei.

Well-defined NMR spectra are analogously shown by the other QBT-*x*-OO molecules. This evidence leads to the hypothesis that in QBT-x-OO species a sole equilibrium ground-state isomer exists. The QBT-x-OO quinoidal character, which is expected to disable isomerization in the ground state, steric hindrance of the alkoxy group, as well as the oxygen−sulfur interactions can be invoked to rationalize this hypothesis.

^{13}C NMR gives consistent observations, with QBT-*x*-OO molecules showing well-defined spectra, whereas just a few very weak signals were detected for biradicaloid QBTs, in analogy to what was previously observed for other quinoidal oligothiophenes.[6]

Ground-State Stability and Equilibrium Molecular Structures. For each molecule in the first row of Figure 1, we performed B3LYP/6-31G** closed-shell (CS) geometry optimization of the ground state (S_0); on the S_0-CS optimized geometry, we further checked the wave-function stability at the (U)B3LYP broken symmetry (BS) level.[4,8,9] If a wave-function instability is found, we fully optimized the molecular structure at the (U)B3LYP(BS) level. As above cited, for QBT-tbu-HH a biradicaloid S_0-BS ground state has been calculated as more stable than the quinoidal S_0-CS one, with a stabilization energy $\Delta E = (S_0(BS) - S_0(CS)) = -0.94$ kcal/mol and a spin contamination of the resulting wave-function $\langle S^2\rangle = 0.67$. Carrying out the same analysis on QBT-tbu-HO, we found that the introduction of the methoxy group on the bithienylene affects the stability of the biradicaloid structure with respect to the quinoidal one. In particular, the electron-donor ability of the methoxy group destabilizes the biradicaloid form, thus reducing ΔE with respect to S_0-CS ($\Delta E = -0.18$ kcal/mol with $\langle S^2\rangle = 0.35$).[43] The addition of a second electron-donor group on the bithiophene core (i.e., QBT-tbu-OO) completely suppresses the biradicaloid character, and no wave-function instability (BS) is found. As a consequence, QBT-tbu-OO results to be fully quinoidal ($\langle S^2\rangle = 0$).[44] An interesting issue is the analysis of the optimized equilibrium geometries of QBT-tbu-Y derivatives. In Figure 3a, we plot the DFT optimized bond lengths of the carbon−carbon bonds along the π-electron conjugation path (excluding the capping C═O bonds for which small variations have been calculated). As has been already discussed,[8] QBT-tbu-HH is characterized by a remarkable bond length equalization in the central part of the bithiophene unit by moving from the quinoidal S_0-CS to the more stable biradicaloid S_0-BS structure. On the contrary, for QBT-tbu-HO, which shows a biradicaloid character less marked than that QBT-tbu-HH, the bond length alternation (BLA) for the stable S_0-BS structure is maintained even in the central part of the molecule, but, in analogy with QBT-tbu-HH, it appears to be reduced. In Figure 3b, the bond length difference between S_0-BS and S_0-CS optimized structures for QBT-tbu-HO ($R_{S0\text{-}BS} - R_{S0\text{-}CS}$) is reported. We can observe that, as it happens for QBT-tbu-HH,[8] the structural relaxations mainly involve the bithiophene unit and the phenone−thiophene inter-ring bonds, thus localizing the biradicaloid character in the central part of the molecule. For the case of QBT-tbu-OO, where a quinoidal (S_0-CS) instead of a biradicaloid structure has been predicted,

dx.doi.org/10.1021/ja3072385 | J. Am. Chem. Soc. 2012, 134, 19070−19083

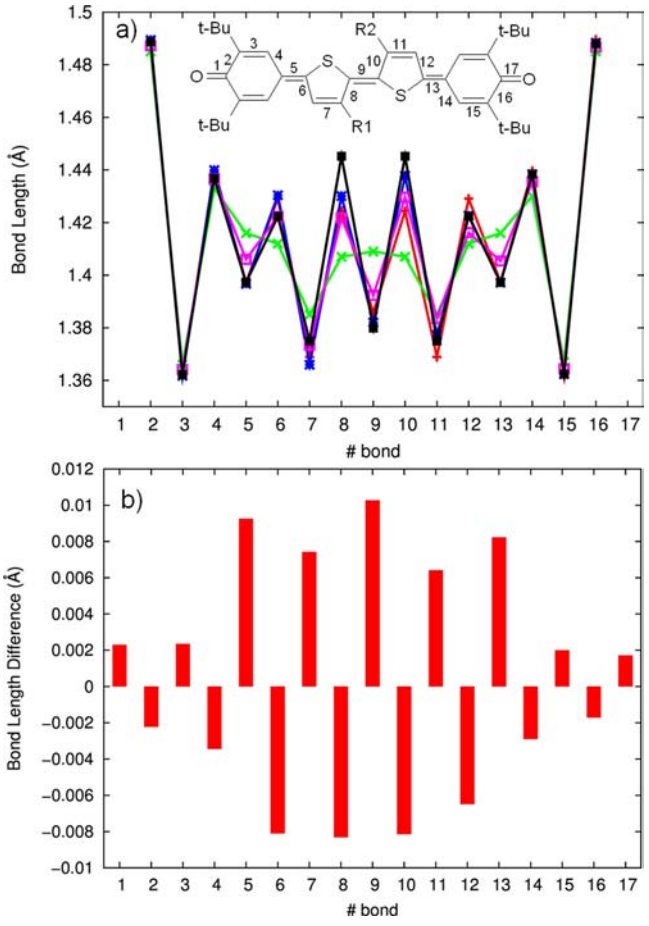

Figure 3. (a) (U)B3LYP/6-31G** bond lengths (Å) for QBT-tbu-HH S_0-CS (red line) and S_0-BS (green line), for QBT-tbu-HO S_0-CS (blue line) and S_0-BS (purple line), and for QBT-tbu-OO S_0-CS (black line). Bond numbers run along the molecular backbone (see molecular sketch). (b) Bond length difference ($R_{S0\text{-}BS} - R_{S0\text{-}CS}$) for QBT-tbu-HO.

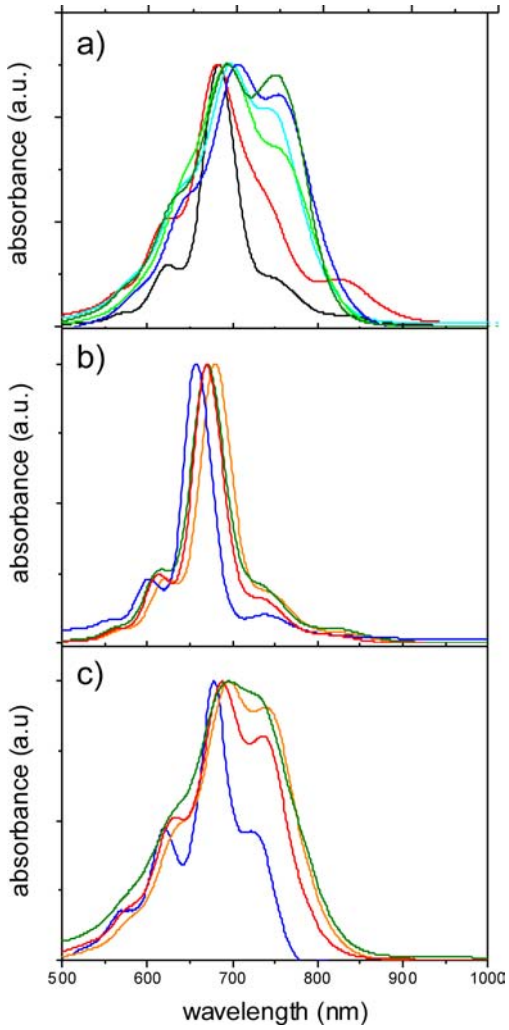

Figure 4. (a) UV–vis absorption spectra in chloroform of QBT-tbu-HH (black line), QBT-tbu-HO (red line), QBT-tbu-OO (light blue line), QBT-ipr-OO (blue line), QBT-me-OO (light green line), and QBT-H-OO (green line); and UV–vis absorption spectra (b) of QBT-tbu-HH and (c) of QBT-tbu-OO in different solvents, *n*-hexane (blue line), THF (red line), chloroform (orange line), and ethanol (green line).

CC bond lengths show a strong alternation pattern, with a quasi double CC bond (bond 9 in Figure 3a) connecting the two thiophene rings.

We can finally state that the introduction of electron-donor groups on the thienylenic core results in a destabilization of the S_0-BS biradicaloid structure, thus favoring the quinoidal S_0-CS character.

UV–Visible Absorption Spectroscopy. Experimental UV–vis spectra have been recorded from dilute chloroform solutions ($<10^{-5}$ M), which is a good solvent for all of the molecules under investigation, thus allowing a direct comparison (Figure 4).

All QBT species show similar absorption features dominated by:

(i) a strong absorption peak in the region of 650–700 nm, which is assigned (see discussion below) to the strongest dipole allowed transition, described in terms of one-electron excitations and characterized by a large HOMO–LUMO contribution.

(ii) a lower energy feature in the range of 750–800 nm assigned to a transition to a state with a dominant double excitation character, which is formally forbidden in dipole approximation as far as it is weakly coupled with single excitations.

(iii) a marked vibronic structure at energy higher than the main absorption band.

While the main peak shows a modest red shift as a consequence of the addition of two donor groups, the general shape of the absorption feature shows a clear evolution, mainly due to the intensity increase of the lower energy transition lead by the addition of the alkoxy groups. On the other hand, the effect of the alkyl groups is less significant: QBT-(x)-OO species only differ in the relative intensity of the low energy band, while the frequency position of the absorption maxima is almost constant.

Polarity of the solvent has a non negligible effect on the spectral pattern: as shown in Figure 4b and 4c for two representative cases, QBT-tbu-HH and QBT-tbu-OO, an increasing solvent polarity determines a batochromic shift of the whole absorption pattern and an intensity increase of the lower energy shoulder. However, while the latter effect is weak for QBT-tbu-HH, it is strongly emphasized in the presence of the alkoxy substituents.

dx.doi.org/10.1021/ja3072385 | J. Am. Chem. Soc. 2012, 134, 19070–19083

Experimental UV−vis spectra of dilute solutions (<10^{-5} M) in an apolar solvent, *n*-hexane, have been also considered, to better simulate a condition of isolated molecules (see Figure 5a, where spectra of the molecules QBT-me-OO and QBT-H-OO are not reported due to their poor solubility in *n*-hexane). Spectra in hexane allow a more convenient comparison with TDDFT simulations (Figure 5b) in vacuo and will be analyzed in deeper detail making explicit reference to the theoretical results. Also, in this case, we detected strong transitions in the red spectral region (650−700 nm) with a vibronic structure at energy higher than that of the absorption maxima, and a transition at lower energy assigned to a state with double excitation character, while no absorption features are recorded after 1000 nm, down to 3000 nm.

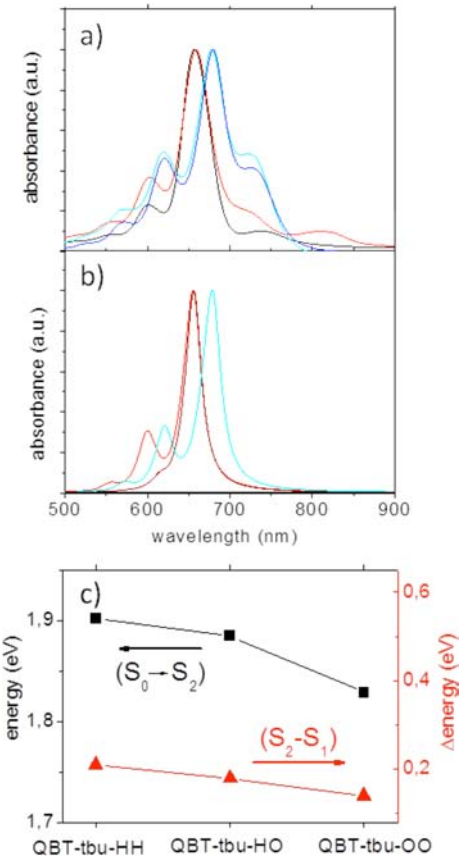

Figure 5. (a) UV−vis absorption spectra in *n*-hexane of QBT-tbu-HH (black line), QBT-tbu-HO (red line), QBT-tbu-OO (light blue line), and QBT-ipr-OO (blue line); (b) TDB3LYP/6-31G** calculated absorption spectra for QBT-H-HO and QBT-H-OO (light blue line); for the first species, both S_0-CS (red line) and S_0-BS (dark red line) geometries have been considered in the calculation of the FC activities; and (c) diagram of the relative positions of the higher wavelength absorption bands for QBT-tbu-HH, QBT-tbu-HO, and QBT-tbu-OO.

The progression of vibronic peaks is very clear in these spectra and becomes more intense by increasing the number of lateral alkoxy chains. As was previously reported,[14] for QBT-tbu-HH the vibronic progression related to the strong, sharp absorption band at 658 nm has been well reproduced and fully rationalized by calculating the TDDFT Franck−Condon (FC) activities for the $S_0 \rightarrow S_2$ transition (S_2 is the dipole allowed excited state, mainly described as HOMO→LUMO transition); weaker bands at higher wavelength have been ascribed to the existence of a low-lying dark double exciton state (named S_1) vibronically coupled to the ground biradicaloid state, as calculated with high level CASPT2 method.[14]

The recognition of double exciton states in the whole series of QBT molecules here considered is relevant, because it is expected to play a fundamental role in ruling the photophysics of organic compounds being determinant in processes such as singlet fission, triplet−triplet annihilation, and conical intersections, as was widely discussed in refs 45−48.

For QBT-tbu-HO, the main absorption band assigned to the $S_0 \rightarrow S_2$ transition slightly changes its energy with respect to QBT-tbu-HH (red-shift ≈ 6 nm). The vibronic progression related to the FC factors of these QBT derivatives is quite similar, with small changes in the relative intensities of the vibronic peaks. This result remarks the likeness of the electronic structure of these two molecules for both the ground and the excited (dipole allowed S_2) states. The absorption features at low energy, which are assigned to a double exciton (S_1) state in analogy with the previous study,[14] characterize both species, with a stronger intensity for QBT-tbu-HO.[49]

For the fully quinoidal QBT-(x)-OO (with (x) = tbu, ipr, me, H), the absorption spectra present (i) a red-shift (∼25 nm) of the main absorption band with respect to the previous cases, and (ii) a blue-shift and an intensity increase of the low energy band, which can be assigned to a transition to a double exciton state, on the basis of the remarkable analogies with another fully quinoidal compound, referred as 2P-**1**T as reported in ref 14. 2P-**1**T is characterized by the same structure as QBT-tbu-HH, while featuring only one thiophene ring. Indeed, the UV−vis spectrum of 2P-**1**T presents an intense absorption band ($S_0 \rightarrow S_2$) characterized by a vibronic structure and a close lower energy strong band assigned to an excited state of a different nature, a double excitation state showing a non-negligible coupling with single excitations.

These findings definitely prove the similarity between polyenic molecules[50,51] and QBT species, which are characterized by the presence of a low-lying double exciton state independently from the character (quinoidal or biradicaloid) of their ground state.

To get further insights into the excited-state energies (both single and double exciton states), we carefully measured the wavelengths corresponding to all of the absorption lines by means of the analysis of the negative second derivative of the absorption spectra, which makes evident the minor transitions, often appearing as shoulders[52] (the detailed analysis is reported in the Supporting Information). For each QBT-tbu-Y derivative (row 1 in Figure 1), the energy difference between the vibrational levels associated with the main electronic transition (e.g., $S_0 \rightarrow S_2$ main absorption band and high energy shoulders) sets on a constant value of about 0.18 eV, consistent with a vibronic progression. Conversely, the lower energy band ($S_0 \rightarrow S_1$) shows a gradual decrease of its distance from the main absorption band ($S_0 \rightarrow S_2$) while increasing the number of alkoxy substituents on the thienyl skeleton. The results are summarized in Figure 4c, where the experimental energy of the main absorption band ($S_0 \rightarrow S_2$ 0−0 transition) and the energy difference between the lowest band ($S_0 \rightarrow S_1$) and the $S_0 \rightarrow S_2$ 0−0 transition are reported. In conclusion, the data collected for the newly synthesized species, besides being perfectly consistent with the experimental finding previously reported, show that the effect of the electro-donor groups is to lower the energy of S_2 and increase that of S_1.

dx.doi.org/10.1021/ja3072385 | J. Am. Chem. Soc. 2012, 134, 19070−19083

TDDFT calculations (both B3LYP and CAM-B3LYP functionals) have been carried out to compute the vertical excitations and to optimize the molecular geometry in the dipole allowed excited state, as well as to calculate its force field (see also the Supporting Information).[53]

TDDFT FC activities have been computed by projecting the excited-state geometry on both S_0-CS and S_0-BS ground-state structures obtained for the biradicaloid QBT-H-HO species, whereas, for the quinoidal QBT-H-OO, only the S_0-CS ground-state structure has been considered (see the Supporting Information for details).[54] The calculated absorption spectra (normalized on the main absorption peak) are reported in Figure 5b. We can observe that for the case of QBT-tbu-HO the intensities of the vibronic progression, calculated considering the S_0-BS (biradicaloid) DFT geometry, are underestimated with respect to the experimental ones; on the contrary, the FC activity is overestimated when the ground S_0-CS geometry is used in the calculation. These findings are parallel to what we have already reported for QBT-tbu-HH[14] and can be related to the difficulty in giving a quantitatively reliable description of the biradicaloid ground-state geometry, which is probably a weighted average between the predicted DFT S_0-CS and S_0-BS structures. Indeed, for the case of the fully quinoidal QBT-tbu-OO, the absorption spectrum related to the strongly dipole allowed transition is well reproduced by TDDFT calculations in terms of FC progression. We found some minor differences by evaluating both ground and excited states using either TDB3LYP or TDCAM-B3LYP methods: in particular, the latter predicts a more pronounced bond length alternation (both in the ground and in the excited states), increasing the relative intensity of the FC progression (further details in the Supporting Information).[55,56]

In the frame of the TDDFT method, it is impossible to describe the lower energy double exciton state: while a possible computational strategy to gain insights in the nature of this state should be to use the CASPT2 method, due to the high computational cost, it is unfeasible for the current study, and the $S_0 \rightarrow S_1$ transition is assigned on the basis of empirical correlations.

Raman Spectroscopy. In this study, we applied the same approach developed for QBT-tbu-HH[8] to investigate the new series of QBT species, with the double aim (i) to provide further insights into their electronic nature and (ii) to confirm the validity of the theoretical and computational methods we have used so far.[8] The analysis is first focused on the most intense Raman feature, assigned to the so-called Я-mode, describing the oscillation of the BLA parameter.[8,13,57] Subsequently, we discuss also weaker spectral features, to better support and to accomplish the vibrational analysis.

QBT-tbu-HH and QBT-tbu-HO present similar Raman spectra with the most intense peak in the 1800−900 cm^{-1} region located at ∼1300 cm^{-1} (Figure 6). As demonstrated before for QBT-tbu-HH,[8] the anomalously low frequency (∼1300 cm^{-1}) of the Я-mode can be justified only taking into account a biradicaloid ground-state structure. The similarity in the main Raman features between QBT-tbu-HH and QBT-tbu-HO spectra further validates the fact that also QBT-tbu-HO has a ground state with a biradicaloid nature, as previously stated on the basis of the predicted stabilization energies and DFT-BS calculations.

Interestingly, the Raman spectra of these two molecules present several bands of comparable intensity: in particular, remarkable features are shown in the 1500−1350 cm^{-1} range

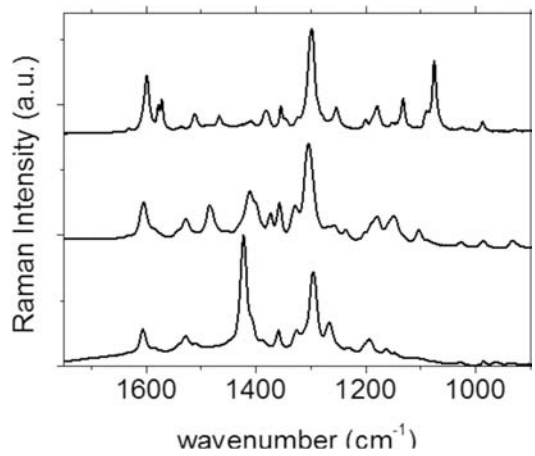

Figure 6. FT-Raman spectra (powder samples) of QBT-tbu-HH (top), QBT-tbu-HO (middle), and QBT-tbu-OO (bottom).

for QBT-tbu-HO and at about 1060 cm^{-1} for QBT-tbu-HH. The Raman spectrum of QBT-tbu-OO is markedly different: indeed, the 1800−900 cm^{-1} spectral region is more selective than in the previous cases and shows the strongest band, assigned to the Я-mode, at 1430 cm^{-1}, up-shifted by more than 100 cm^{-1} with respect to the Я-mode transition of the biradicaloid species. The occurrence of a Я-mode at higher energy confirms that QBT-tbu-OO has a quinoidal ground state, as further confirmed by DFT-BS calculations.

In Figure 7, we report the calculated DFT Raman spectra for the newly synthesized compounds QBT-tbu-HO (Figure 7a) and QBT-tbu-OO (Figure 7b). In particular, for QBT-tbu-HO, the experimental FT-Raman spectrum is compared to DFT predictions obtained according to the following procedures: (i) standard method, by using the S_0-CS (B3LYP) equilibrium structure and wave-function, (ii) S_0-BS (UB3LYP) equilibrium structure and CS wave-function, (iii) both structures and wave-functions at S_0-BS level, and, finally, (iv) adopting a fictitious geometry, obtained after displacing the nuclei along the Я-mode coordinate,[8] in conjunction with CS wave-function.

Method (i) does not reproduce the Raman spectra, because it predicts the Я-mode (stronger line) frequency about 100 cm^{-1} higher than the experimental one. This result was expected, because the biradicaloid S_0-BS structure is more stable (ΔE = −0.18 kcal/mol) than the S_0-CS quinoidal one. We thus adopted approaches (ii) and (iii). Approach (ii) takes into account only the nuclear effect of the molecular geometry (S_0-BS structure instead of S_0-CS (see Figure 3)), whereas approach (iii) explicitly considers the electronic effects provided by the electron charge distribution typical of the biradicaloid structure. In case (ii), the calculated Raman spectrum is similar to that obtained with the fully S_0-CS approach, showing a few strong band with a high energy Я-mode at 1410 cm^{-1}. Conversely, case (iii) gives a very different result: the computed Raman spectrum presents many strong Raman transitions (especially in the region 1600−1400 cm^{-1}), and the Я-mode is red-shifted at 1305 cm^{-1}, in good agreement with the experimental frequency value (1300 cm^{-1}). Moreover, at 1600 cm^{-1}, the calculated Raman spectrum shows, as the experimental one, a doublet of peaks, due to the splitting of the quasi-degenerate C═O stretching modes of the two carbonyl groups. The occurrence of this doublet in the Raman spectrum further supports the biradicaloid character; in fact, it is also present in the Raman spectrum of QBT-tbu-HH, but it is

dx.doi.org/10.1021/ja3072385 | J. Am. Chem. Soc. 2012, 134, 19070−19083

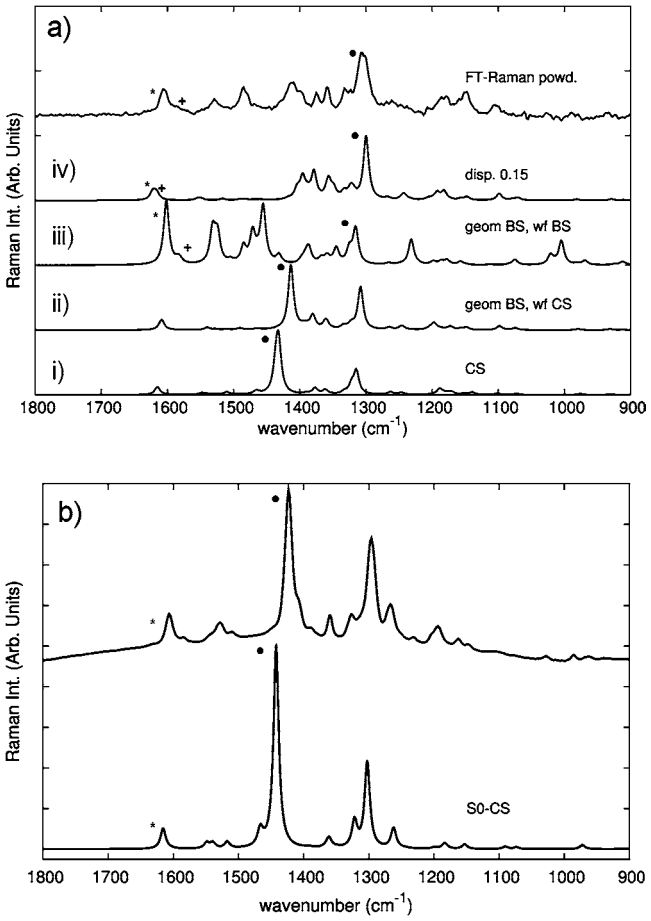

Figure 7. (a) Calculated B3LYP/6-31G** Raman spectra for QBT-tbu-HO evaluated with (i) S_0-CS geometry and wave-function, (ii) S_0-BS (UB3LYP) geometry and CS wave-function, (iii) S_0-BS geometry and wave-function, and (iv) a displaced geometry (along the Я-coordinate) with CS wave-function. The experimental FT-Raman spectrum is reported as comparison. Calculated frequencies have been scaled by a factor 0.96814. (b) B3LYP/6-31G** S_0-CS calculated Raman spectra for QBT-tbu-OO (below) and the experimental one (above). Calculated frequencies have been scaled by a factor of 0.96814.

absent in that of QBT-tbu-OO (see Figure 6). However, the prediction of the Raman spectrum according to case (iii) is necessarily affected by the intrinsic weakness of the DFT theory in the description of multireference systems, giving spin-contaminated wave-functions: we may ascribe to this flaw the inaccuracy of our calculation in the prediction of the intensity pattern, giving an underestimation of the intensity of the Я-mode and a general overestimation of the Raman activity in the 1450−1550 cm^{-1} region (see Figure 7a).

A strategy we have already adopted to correctly reproduce the Raman spectra of biradicaloid systems[8] is the study of the dependence of the Raman spectrum on the nuclear geometry: a modulation of the molecular structure starting from the (mainly quinoidal) S_0-CS equilibrium geometry toward a more aromatic (biradicaloid) one[7−9] is obtained by displacing nuclei along the Я-coordinate. The Raman spectrum (computed with the S_0-CS wave-function) is subsequently calculated at different frozen nuclei geometries, corresponding to increasingly large displacements. In Figure 7a, we report the spectrum of QBT-tbu-HO, obtained after a nuclear displacement of $\Delta Я = 0.15$ A/amu^2; a very good agreement with the experimental spectrum is achieved, the Я-mode being correctly predicted in terms of both frequency and relative intensity; moreover, also the doublet at 1600 cm^{-1} is nicely reproduced. It is worthwhile noting that the remarkable modulation of the Raman spectrum obtained by the above procedure provides an independent proof of the existence of a large electron−phonon coupling, occurring along the Я direction.

Figure 7b compares the calculated B3LYP/6-31G** Raman spectrum of QBT-tbu-OO and its FT-Raman experimental counterpart. In this case, the prediction by standard procedure is in good agreement with the experimental spectrum, with the Я-mode at 1420 cm^{-1} resulting as the most intense Raman peak in the 1800−900 cm^{-1} region.

Concerning the minor Raman features, QBT-tbu-OO shows an interesting pattern in the 1370−1300 cm^{-1} region. These peaks can be related to the different dynamical coupling between the molecular backbone vibrations and those of the alkyl groups attached onto the phenone. Indeed, by reducing their hindrance (tbu→ipr→me) toward the unsubstituted species QBT-H-OO, we observed a variation of the spectral pattern and relative intensities in the region 1200−1400 cm^{-1} (as reported in the experimental spectra of Figure 8a), while the 1440 cm^{-1} band, which is related to the Я-mode, remains almost unaffected.

The spectral patterns in the 1500−1350 cm^{-1} region are nicely reproduced by the calculated Raman spectra, as reported in Figure 8a. In Figure 8b, the normal modes for the Raman active bands (red arrows) around 1300 cm^{-1} are sketched. Specifically, CC and CS bond stretching of the molecular backbone are coupled to the CH bending of phenone and thiophene rings and also to the CH_2 waggings of the alkoxy chains. We observe that by changing the capping phenone, a different dynamical coupling takes place between a Я-like oscillation, involving the CC bonds in the molecular backbone and displacements localized on the end groups, resulting in a modulation of frequencies and relative Raman intensities.

Finally, following the recent works by Navarrete et al.[9,24] dealing with other quinoidal thiophene-based series, the thermal evolution of the Raman spectra can be analyzed to discuss the possible presence of low energy species, as for instance low-lying triplet states, which can show non-negligible population already at room temperature.

In the Supporting Information, Raman spectra of QBT-tbu-HH and QBT-tbu-OO recorded at different temperatures (−190 to 80 °C) are reported. In the case of QBT-tbu-OO, the observed spectra evolution with increasing temperature can be described in terms of a general broadening and frequency shift of the Raman bands (which is usually ascribed to the increased molecular mobility), without clear indication of the presence of different molecular species characterized by a thermally modulated relative population. The spectra evolution shown by QBT-tbu-HH is much more intriguing because it is possible to detect (Figure 9) a peculiar evolution of the structured band at about 1060 cm^{-1}, which shows an asymmetric shape already at −190 °C, resulting in a shoulder on the lower frequency side at increasing temperatures. At $T = 0$ °C, the small but clear shift of the maximum frequency ($\Delta\nu \cong 1$ cm^{-1}) can be interpreted as the result of the convolution of the two components, which contributes to the Raman bands with comparable weights, while the further peak shift at higher temperature, accompanied by remarkable band broadening, may be ascribed to effects related to thermal expansion. These experimental findings suggest that in the QBT-tbu-HH sample, a molecular species different from

dx.doi.org/10.1021/ja3072385 | J. Am. Chem. Soc. 2012, 134, 19070−19083

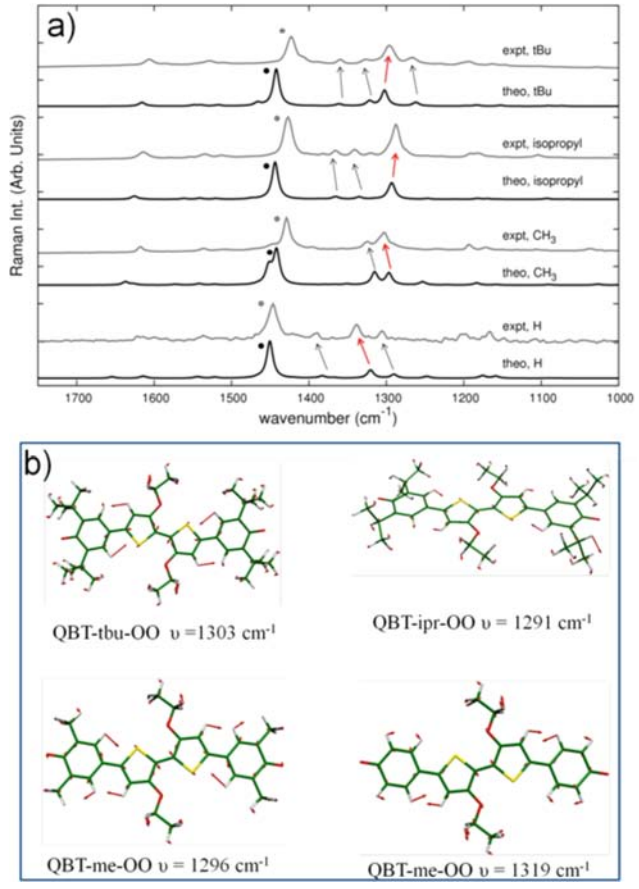

Figure 8. (a) Experimental (gray lines) and theoretical (black lines) Raman spectra for QBT-(x)-OO species (from the bottom, (x) = H, me, ipr, tbu). Black and gray circles indicate the Я-mode; arrows indicate the correspondences between theoretically predicted and experimental bands. Red arrows indicate one of the most intense Raman peaks around 1300 cm^{-1}. (b) Calculated normal modes for QBT-(x)-OO relative to the Raman peaks indicated by the red arrows in panel (a).

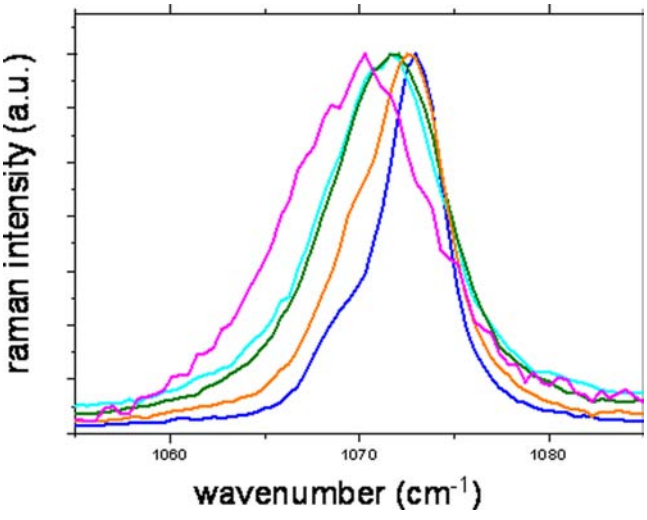

Figure 9. Raman spectra of QBT-tbu-HH with temperature: −190 °C (blue line), −110 °C (orange line), −30 °C (green line), 0 °C (cyan line), and 80 °C (magenta line).

the lower energy one occurs. However, on the basis of this evidence, it is difficult to assign the observed rise of the lower frequency component of the 1060 cm^{-1} band to the occurrence of molecules in a triplet state. The computed Raman spectra of triplet states species (see the Supporting Information) do not support this finding, and further experimental and theoretical investigations will be necessary for a reliable assignment.

Multiwavelength Raman Scattering. The spectroscopic characterization has been extended to the study of the Raman spectral pattern evolution while changing the laser excitation line (λ_{exc}). The experimental FT-Raman spectra presented in the previous section were recorded by exciting at λ_{exc}= 1064 nm, to avoid resonance phenomena with the strong dipole allowed electronic transitions of QBTs ($\lambda_{abs} \approx 700$ nm). λ_{exc} at higher energy approaches the absorption band of QBTs, possibly matching the resonance condition. Two different radiations were chosen with photon energy nearly in correspondence (λ_{exc} = 632 nm) or above (λ_{exc} = 514 nm) the main electronic transition of QBTs.

In Figure 10, the spectra of QBT-tbu-YY, obtained by exciting at different λ_{exc}, are reported: as first evidence, the most intense Raman band, assigned to the Я-mode, still dominates the spectra, thus confirming that this peculiar vibration has an intrinsically very strong Raman activity.

Nevertheless, looking at the intensity pattern, some non-negligible changes are detected especially for the two molecules featuring a biradicaloid character, while QBT-tbu-OO spectrum is quite insensitive to the excitation energy. The intensity pattern variations have opposite trends in different spectral regions: in the region 1000−1200 cm^{-1}, where normal modes are more localized onto the thiophene rings, band intensities raise by increasing the excitation energy; on the opposite, transitions associated with normal modes at higher wavenumbers (e.g., 1600 cm^{-1}) mainly involving the phenones weaken.

This experimental evidence can find a qualitative explanation in the frame of the Albrecht theory of the Raman scattering.[58,59] When dealing with polyconjugated molecules characterized by a low energy strongly dipole allowed excited state, named "e" state, both nonresonant and resonant Raman spectra are dominated by the contribution of this relevant excited state (e). If state "e" is characterized by a remarkable relaxation of the equilibrium geometry, the general intensity pattern can be predicted simply considering the so-called *A* term,[60] ruled by the change of the equilibrium molecular structure ($\Delta X^{e,g}$) while passing from the ground (g) to the relevant excited state (e). As a consequence, those normal modes (Q_i) describing a nuclear trajectory with a non-negligible projection ($\Delta Q_i^{e,g}$) on $\Delta X^{e,g}$ show a remarkably high Raman activity, and the resulting Raman spectrum is strong and very selective, independently on the matching of the resonance condition with state "e". In other words, resonant and non resonant Raman patterns are similar each other, as it has been described since long time in the case of polyenes.[13] In this framework, the origin of the strong intensity of Я-mode can be justified as follows: the relaxation of the nuclear geometry in the relevant excited state "e" usually implies a decrease of the BLA, giving a structural reorganization parallel to the Я-mode displacements, thus enhancing the *A* term. Conversely, when the geometry displacement $\Delta X^{e,g}$ is small, the *A* term is not further dominant, and additional contributions to the Raman activity must be taken into consideration; in addition, contributions from states different from "e" could become of comparable importance. For this reason, a weaker and less selective Raman spectrum is expected,

dx.doi.org/10.1021/ja3072385 | J. Am. Chem. Soc. 2012, 134, 19070−19083

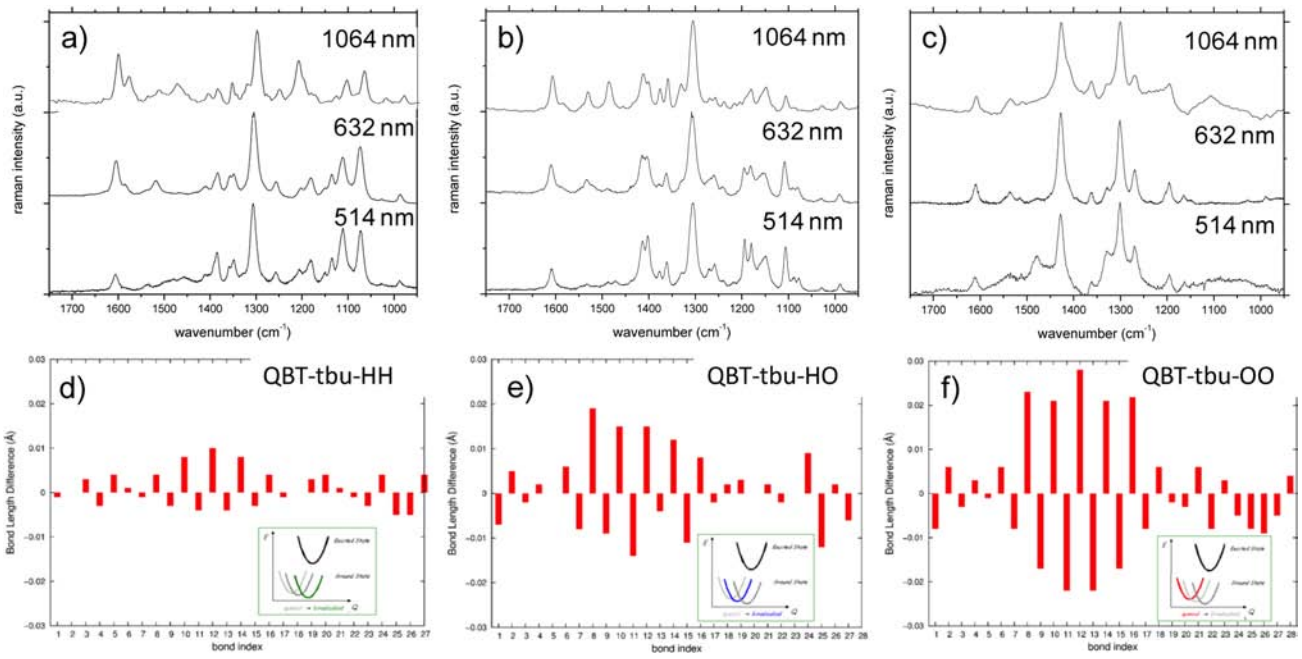

Figure 10. Top: Raman spectra of (a) QBT-tbu-HH; (b) QBT-tbu-HO; and (c) QBT-tbu-OO in chloroform solution, recorded by exciting at 1064 nm (top), 632 nm (middle), and 514 nm (bottom). Bottom: Bond length differences between the TDDFT optimized geometries of the dipole allowed excited state S_2 and the stable ground state, of (d) QBT-tbu-HH; (e) QBT-tbu-HO; and (f) QBT-tbu-OO.

possibly showing a complex evolution while varying the excitation energy.

To verify the reliability of the qualitative interpretation suggested above, we consider (see Figure 10, bottom) the differences of the equilibrium bond lengths along the conjugated sequence of CC bonds, as obtained considering the TDDFT optimized geometry of the S_2 state and that of the more stable ground state ($R_{S2} - R_{S0}$), for the three molecules under investigation (QBT-H-OO (S_0-CS), -HO (S_0-BS), and -HH (S_0-BS)).

QBT-H-OO shows the largest bond length differences between the excited and the ground states ($\Delta X^{e,g}$), whereas for QBT-H-HO and QBT-H-HH, $\Delta X^{e,g}$ decreases by increasing the biradicaloid ground-state character. According to the qualitative description given above (i.e., large $\Delta X^{e,g}$ with high projection $\Delta Q_i^{e,g}$ over Я coordinates), in the case of QBT-H-OO the general Raman pattern is well reproduced through the calculation of the Franck−Condon factors for all of the Raman active normal vibrations (see the Supporting Information).

On the opposite side, QBTs showing a biradicaloid electronic ground state are characterized by an equalized sequence of CC bonds along the conjugation path (small BLA) also in the ground state, thus featuring lower $\Delta X^{e,g}$ with respect to QBT-H-OO. As a result, the Raman spectrum cannot be simply interpreted only on the basis of term *A*; other contributions have to be taken into account. The consequence is that the Я-mode is not the only mode dominating the Raman spectrum, but other modes are activated, thus featuring spectra of biradicaloid QBTs less selective than for the quinoidal species and more affected by dispersion while changing the excitation energy. This effect is usually accompanied by a general weakening of the Raman activity, which no longer benefits the (usually large) contribution from term *A*. Experiments confirm this behavior because Raman spectra recorded at the same laser power are weaker and noisier in the case of molecules characterized by a biradicaloid ground state.

CONCLUSIONS

New thiophene-based heteroquaterphenoquinones have been synthesized with bulky to less steric demanding alkyls on the 3,5-positions of the phenoquinone and/or alkoxy groups on the bithienylene core.

Spectroscopic characterization highlighted a strong contribution of the donor substituents in stabilizing the quinoidal ground-state structure of these species and provided the identification of markers of their electronic structure. Specifically, quinoidal electronic structures, with respect to biradicaloid ones, show (i) a displacement toward higher energy and an intensity increase of the absorption band associated to the double exciton state, at lower energy with respect to the strongly dipole allowed excited state, mainly described by a single (HOMO−LUMO) excitation; (ii) a sharpening of the ^{1}H NMR signals in the region 6−8 ppm; and (iii) a remarkable shift of 100 cm^{-1} observed for the strongest Raman band assigned to the Я-mode. Raman spectra have been successfully predicted, also when dealing with the subtle changes of the Raman pattern associated with the presence of differently hindered phenones, which indeed require a reliable description of the vibrational couplings.

From the characterization of this homologous series of molecules, it followed that, while maintaining the same oligomer length, a perturbation of the π-electron distribution of the conjugated main molecular axis by introducing side donor groups turns into a strong stabilization of the quinoidal electronic structure, with a negligible decrease of the energy gap. This represents a new insight into the general class of thiophene-based quinoidal molecules, where only the dependence of the biradicaloid structure on the effective conjugation length (e.g., E_{gap}) has been so far deeply characterized.

dx.doi.org/10.1021/ja3072385 | J. Am. Chem. Soc. 2012, 134, 19070−19083

■ ASSOCIATED CONTENT

Supporting Information

NMR spectra, analysis of absorption spectra (second derivatives), cyclic voltammetry measurements, DFT, TDDFT, CASSCF(12,12) optimized geometries and absolute energies for QBT-x-YY, IEFPCM optimized geometries and absolute energies, TDDFT computed Franck−Condon factors, FT-Raman spectra of solution and solid-state samples, temperature-dependent Raman spectra, computed Raman spectrum of the triplet state of QBT-tbu-HH, and computed TDDFT resonant Raman spectrum of QBT-H-OO. This material is available free of charge via the Internet at http://pubs.acs.org.

■ AUTHOR INFORMATION

Corresponding Author

eleonora.canesi@iit.it

Notes

The authors declare no competing financial interest.

■ ACKNOWLEDGMENTS

This work has been partially supported by Fondazione Cariplo, grant no. 2011-0368, and by the Italian Scientific and Technological Research Ministry through PRIN project no. 2008JKBBK4_003.

■ REFERENCES

(1) Takahashi, K.; Gunji, A.; Yanagi, K.; Miki, M. *J. Org. Chem.* **1996**, *61*, 4784.

(2) Abbotto, A.; Bradamante, S.; Facchetti, A.; Pagani, G. A. *J. Org. Chem.* **1997**, *62*, 5755.

(3) Casado, J.; Miller, L. L.; Mann, R. K.; Pappenfus, T. M.; Higuchi, H.; Orti, E.; Milian, B.; Pou-Amerigo, R.; Hernandez, V.; Navarrete, L. T. J. *J. Am. Chem. Soc.* **2002**, *124*, 12380.

(4) Pappenfus, T. M.; Chesterfield, R. J.; Frisbie, D. C.; Mann, R. K.; Casado, J.; Raff, D. J.; Miller, L. L. *J. Am. Chem. Soc.* **2002**, *124*, 4184.

(5) Berlin, A.; Grimoldi, S.; Zotti, G.; Osuna, M. R.; Delgado, R. C. M.; Ortiz, P. R.; Casado, J.; Hernandenz, V.; Navarrete, L. T. J. *J. Phys. Chem. B* **2005**, *109*, 22308.

(6) Takahashi, T.; Matsuoka, K. I.; Takimiya, K.; Otsubo, T.; Aso, Y. *J. Am. Chem. Soc.* **2005**, *127*, 8928.

(7) Casado, J.; Ortiz, R. P.; Navarrete, L.T. J. *Chem. Soc. Rev.* **2012**, *41*, 5672.

(8) Fazzi, D.; Canesi, E. V.; Negri, F.; Bertarelli, C.; Castiglioni, C. *ChemPhysChem* **2010**, *11*, 3685.

(9) Ponce Ortiz, R.; Casado, J.; Rodriguez Gonzales, S.; Hernandez, V.; Navarrete, L. T.; Viruela, P. M.; Ortì, E.; Takimiya, K.; Otsubo, T. *Chem.-Eur. J.* **2010**, *16*, 470.

(10) Ribierre, J.-C.; Watanabe, S.; Matsumoto, M.; Muto, T.; Nakao, A.; Aoyama, T. *Adv. Mater.* **2010**, *22*, 4044.

(11) Suzuki, Y.; Shimawaki, M.; Miyazaki, E.; Osaka, I.; Takimiya, K. *Chem. Mater.* **2010**, *23*, 795.

(12) Ortiz, R. P.; Casado, J.; Hernandez, V.; Navarrete, L. T. J.; Viruela, M. P.; Orti, E.; Takimiya, K.; Otsubo, T. *Angew. Chem., Int. Ed.* **2007**, *46*, 9057.

(13) Castiglioni, C.; Tommasini, M.; Zerbi, G. *Philos. Trans. R. Soc. London, Ser. A* **2004**, *362*, 2425.

(14) Di Motta, S.; Negri, F.; Fazzi, D.; Castiglioni, C.; Canesi, E. V. *J. Phys. Chem. Lett.* **2010**, *1*, 3334.

(15) Smith, M. B.; Michl, J. *Chem. Rev.* **2010**, *110*, 6891.

(16) Paci, I.; Johnson, J. C.; Chen, X.; Rana, G.; Popović, D.; David, D. E.; Nozik, A. J.; Ratner, M. A.; Michl, J. *J. Am. Chem. Soc.* **2006**, *128*, 16546.

(17) Quarti, C.; Fazzi, D.; Del Zoppo, M. *Phys. Chem. Chem. Phys.* **2011**, *13*, 18615.

(18) Agostinelli, T.; Caironi, M.; Natali, D.; Sampietro, M.; Dassa, G.; Canesi, E. V.; Bertarelli, C.; Zerbi, G.; Cabanillas-Gonzalez, J.; De Silvestri, S.; Lanzani, G. *J. Appl. Phys.* **2008**, *104*, 114508.

(19) González, S. R.; Ie, Y.; Aso, Y.; López Navarrete, J. T.; Casado, J. *J. Am. Chem. Soc.* **2011**, *133*, 16350.

(20) Suzuki, Y.; Miyazaki, E.; Takimiya, K. *J. Am. Chem. Soc.* **2010**, *132*, 10453.

(21) Handa, S.; Miyazaki, E.; Takimiya, K.; Kunugi, Y. *J. Am. Chem. Soc.* **2007**, *129*, 11684.

(22) Wu, Q.; Li, R.; Hong, W.; Li, H.; Gao, X.; Zhu, D. *Chem. Mater.* **2011**, *23*, 3138.

(23) Nakano, M.; Kishi, R.; Yoneda, K.; Inoue, Y.; Inui, T.; Shigeta, Y.; Kubo, T.; Champagne, B. t. *J. Phys. Chem. A* **2011**, *115*, 8767.

(24) Ponce Ortiz, R.; Casado, J.; Hernández, V.; López Navarrete, J. T.; Ortí, E.; Viruela, P. M.; Milián, B.; Hotta, S.; Zotti, G.; Zecchin, S.; Vercelli, B. *Adv. Funct. Mater.* **2006**, *16*, 531.

(25) Takahashi, K.; Suzuki, T.; Akiyama, K.; Ikegami, Y.; Fukazawa, Y. *J. Am. Chem. Soc.* **1991**, *113*, 4576.

(26) Zotti, G.; Gallazzi, M. C.; Zerbi, G.; Meille, S. V. *Synth. Met.* **1995**, *73*, 217.

(27) Becke, A. D. *J. Chem. Phys.* **1993**, *98*, 5648.

(28) Yanai, T.; Tew, D. P.; Handy, N. C. *Chem. Phys. Lett.* **2004**, *393*, 51.

(29) Di Donato, E.; Vanzo, D.; Semeraro, M.; Credi, A.; Negri, F. *J. Phys. Chem. A* **2009**, *113*, 6504.

(30) Negri, F.; Orlandi, G. In *Computational Photochemistry*; Olivucci, M., Ed.; Elsevier: New York, 2005; Vol. *16*, p 129.

(31) Negri, F.; Zgierski, M. Z. *J. Chem. Phys.* **1994**, *100*, 1387.

(32) Negri, F.; Zgierski, M. Z. *J. Chem. Phys.* **1994**, *100*, 2571.

(33) Negri, F.; Orlandi, G.; Zerbetto, F. *Chem. Phys. Lett.* **1988**, *144*, 31.

(34) Negri, F.; Orlandi, G. *J. Phys. B: At. Mol. Opt. Phys.* **1996**, *29*, 5049.

(35) Santoro, F.; Improta, R.; Lami, A.; Bloino, J.; Barone, V. *J. Chem. Phys.* **2007**, *126*, 084509.

(36) Santoro, F.; Lami, A.; Improta, R.; Barone, V. *J. Chem. Phys.* **2007**, *126*, 184102.

(37) Barone, V.; Bloino, J.; Biczysko, M.; Santoro, F. *J. Chem. Theory Comput.* **2009**, *5*, 540.

(38) Tomasi, J.; Mennucci, B.; Cammi, R. *Chem. Rev.* **2005**, *105*, 2999.

(39) Mennucci, B.; Cammi, R. *Continuum Solvation Models in Chemical Physics: From Theory to Applications*; Wiley: Chirchester, U.K., 2007.

(40) Frisch, M. J.; et al. *Gaussian 09*, revision A.1; Gaussian, Inc.: Wallingford, CT, 2009.

(41) Valiev, M.; Bylaska, E. J.; Govind, N.; Kowalski, K.; Straatsma, T. P.; Van Dam, H. J. J.; Wang, D.; Nieplocha, J.; Apra, E.; Windus, T. L.; de Jong, W. A. *Comput. Phys. Commun.* **2010**, *181*, 1477.

(42) Lanata, M.; Bertarelli, C.; Gallazzi, M. C.; Bianco, A.; Del Zoppo, M.; Zerbi, G. *Synth. Met.* **2003**, *138*, 357.

(43) We calculated S0-CS and S0-BS optimized structures also for a model molecule QBT-H-HO, carrying hydrogen atoms instead of ^{t}Bu groups on the phenyl moieties, and we found that ΔE is just slightly increased (ΔE = −0.21 kcal/mol with $\langle S2\rangle$ = −0.38).

(44) The same result is obtained from calculation on QBT-x-OO, with x = ipr, me, H.

(45) Zimmerman, P. M.; Bell, F.; Casanova, D.; Head-Gordon, M. *J. Am. Chem. Soc.* **2011**, *133*, 19944.

(46) Barbatti, M. *WIREs: Comp. Mol. Sci.* **2011**, *1*, 620.

(47) Barbatti, M.; Aquino, A. J. A.; Szymczak, J. J.; Nachtigallova, D.; Lischka, H. *Phys. Chem. Chem. Phys.* **2011**, *13*, 6145.

(48) Plasser, F.; Barbatti, M.; Aquino, A. J. A.; Lischka, H. *Theor. Chem. Acc.* **2012**, *131*, 1073.

(49) The transition to S1, described as a double exciton state, is expected to vanish for molecules featuring an inversion symmetry centre (S1 is a dark state). Asymmetries induced by the environment, deviation from the molecular planarity, as well as the introduction of

asymmetric chemical substituents can concur to the activation of the S0−S1 transition.
(50) Orlandi, G.; Zerbetto, F.; Zgierski, M. Z. *Chem. Rev.* **1991**, *91*, 867.
(51) Kohler, B. E.; Spangler, C.; Westerfield, C. *J. Chem. Phys.* **1988**, *89*, 5422.
(52) Hagler, T. W.; Pakbaz, K.; Voss, K. F.; Heeger, A. J. *Phys. Rev. B* **1991**, *44*, 8652.
(53) Despite the fact that biradicaloid species, as QBT-tbu-HH and QBT-tbu-HO, need multireference methods for a reliable description of both ground and excited states, we used here TDDFT calculations as the method is likely accurate for describing dipole allowed excited state characterized by single excitations and shows good performances in evaluating energy gradients and Hessians.
(54) For TDDFT FC calculations, we considered only hydrogen capped QBT species instead of ^{t}Bu due to the computationally demanding evaluation of the force fields in the dipole allowed excited states.
(55) Jacquemin, D.; Planchat, A.; Adamo, C.; Mennucci, B. *J. Chem. Theory Comput.* **2012**, *8*, 2359.
(56) Jacquemin, D.; Mennucci, B.; Adamo, C. *Phys. Chem. Chem. Phys.* **2011**, *13*, 16987.
(57) Fazzi, D.; Canesi, E. V.; Bertarelli, C.; Castiglioni, C.; Negri, F.; Zerbi, G. *J. Raman Spectrosc.* **2010**, *41*, 406.
(58) Albrecht, A. C. *J. Chem. Phys.* **1960**, *33*, 156.
(59) Albrecht, A. C. *J. Chem. Phys.* **1961**, *34*, 1476.
(60) Andruniów, T.; Olivucci, M. *J. Chem. Theory Comput.* **2009**, *5*, 3096.